Fisheries Research 246 (2022) 106169

Contents lists available at ScienceDirect

Fisheries Research

journal homepage: www.elsevier.com/locate/fishres

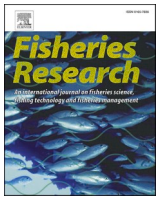

Impacts of fisheries-dependent spatial sampling patterns on catch-per-unit-effort standardization: A simulation study and fishery application

Nicholas D. Ducharme-Barth [a,*,1], Arnaud Grüss [b,2], Matthew T. Vincent [a,3], Hidetada Kiyofuji [c], Yoshinori Aoki [c], Graham Pilling [a], John Hampton [a], James T. Thorson [d]

[a] Pacific Community, 95 Promenade Roger Laroque, B.P. D5 98848, Noumea, New Caledonia
[b] School of Aquatic and Fishery Sciences, University of Washington, Box 355020, Seattle, WA 98105-5020, USA
[c] Fisheries Resources Institute, Japan Fisheries Research and Education Agency, 2–12-4 Fukuura, Kanazawa, Yokohama, Kanagawa 236-8648, Japan
[d] Habitat and Ecological Processes Research Program, Alaska Fisheries Science Center, NOAA, Seattle, WA, USA

ARTICLE INFO

Handled by Dr Steven X. Cadrin

Keywords:
Spatial sampling
Spatiotemporal models
Catch-per-unit-effort (CPUE) standardization
Simulation-testing
Pacific skipjack tuna

ABSTRACT

Abundance indices derived from fisheries-dependent data (catch-per-unit-effort or CPUE) are known to have potential for bias, in part because of the usual non-random nature of fisheries spatial distributions. However, given the cost and lack of availability of fisheries-independent surveys, fisheries-dependent CPUE remains a common and informative input to fisheries stock assessments. Recent research efforts have focused on the development of spatiotemporal delta-generalized linear mixed models (GLMMs) which simultaneously standardize the CPUE and predict abundance in unfished areas when estimating the abundance index. These models can include local seasonal environmental covariates (e.g. sea surface temperature) and a spatially varying response to regional annual indices (e.g. the El Niño Southern Oscillation) to interpolate into unfished areas. Spatiotemporal delta-GLMMs have been demonstrated in simulation studies to perform better than conventional, non-spatial delta-generalized linear models (GLMs). However, spatiotemporal delta-GLMMs have rarely been evaluated in situations where fisheries spatial sampling patterns change over time (e.g. fisheries expansion or spatial closures). This study develops a simulation framework to evaluate 1) how the nature of fisheries-dependent spatial sampling patterns may bias estimated abundance indices, 2) how shifts in spatial sampling over time impact our ability to estimate temporal changes in catchability, and 3) how including seasonal environmental covariates and/or regional annual indices in spatiotemporal delta-GLMMs can improve the estimation of abundance indices given shifts in spatial sampling. Spatiotemporal delta-GLMMs are then applied to a case study example where the spatial sampling pattern changed dramatically over time (contraction of the Japanese pole-and-line fishery for skipjack tuna *Katsuwonus pelamis* in the western and central Pacific Ocean). Results from simulations indicate that spatial sampling in proportion to the underlying biomass can produce similar abundance indices to those produced under random sampling. Though estimated abundance indices were not perfect, spatiotemporal GLMMs were generally able to disentangle shifts in spatial sampling from temporal changes in catchability when shifts in spatial sampling were not too extreme. Lastly, the inclusion of seasonal environmental covariates and/or regional oceanographic indices in spatiotemporal GLMMs did not improve abundance index estimation and in some cases resulted in degraded model performance.

* Corresponding author.
E-mail address: nicholas.ducharme-barth@noaa.gov (N.D. Ducharme-Barth).
[1] Present address: NOAA National Marine Fisheries Service, Pacific Islands Fisheries Science Center, 1845 Wasp Boulevard, Building 176, Honolulu, Hawaii, USA 96818
[2] Present address: National Institute of Water and Atmospheric Research, 301 Evans Bay Parade, Greta Point, Wellington 6021, New Zealand
[3] Present address: Southeast Fisheries Science Center NOAA Beaufort Lab, 101 Pivers Island Rd, Beaufort, NC 28516, USA

https://doi.org/10.1016/j.fishres.2021.106169
Received 15 April 2021; Received in revised form 19 October 2021; Accepted 26 October 2021
Available online 10 November 2021

1. Introduction

Abundance indices derived from fisheries-dependent catch-per-unit-effort (CPUE) remain a common and informative input to fisheries stock assessment models. Despite the known potential for bias, these indices are often assumed to be directly proportional to abundance and provide information to the model on population trend. These biases can arise from the usual non-random nature of the spatiotemporal distribution of fishers relative to that of fish populations ("preferential sampling"; Clark and Mangel, 1979; Rose and Leggett, 1991; Rose and Kulka, 1999; Swain and Sinclair, 1994), gear effects ("saturation of the gear"; Deriso and Parma, 1987), and/or systemic and structural changes to the fishing fleets over time ("effort creep"; Bishop et al., 2004; Ye and Dennis, 2009).

While fisheries-independent data usually come from statistically designed surveys that ensure the random distribution of samples relative to the fish populations, typically defined using a spatial sampling frame (Cochran, 1977; Kotwicki and Ono, 2019), the same assumption of appropriate spatiotemporal coverage cannot be made for fisheries-dependent data. Spatiotemporal "holes" or unfished areas in fisheries-dependent data coverage can arise from sampling preferentially with respect to fish abundance (Pennino et al., 2019), changes in spatial targeting due to economic or management factors driving fishing preferences (Quirijns et al., 2008), or avoidance of target and/or bycatch species (e.g. fisheries under quota management systems; Branch and Hilborn, 2008), as well as restricted access to fishing grounds due to regulatory or competitive forces (Wilen, 2004). These anomalies in spatiotemporal sampling could lead to a disconnect between the underlying species abundance trend and the trend estimated from fisheries-dependent CPUE data, thus providing a biased abundance index. Despite these potential deficiencies and biases, the high-cost and logistical challenges associated with implementing fisheries-independent surveys (Dennis et al., 2015) means that in some cases fisheries-dependent data are the only data available from which to construct relative abundance indices for fisheries stock assessments. Given the risk that fisheries-dependent CPUE can deviate from a proportional relationship with abundance (Harley et al., 2001), considerable research (Campbell, 2004, 2015; Walter et al., 2014a; Grüss et al., 2019; Zhou et al., 2019) has been directed at appropriately standardizing out the aforementioned sources of bias.

The delta-generalized linear model (GLM) is one of the traditional fishery-dependent CPUE standardization approaches. It relies on a two-stage approach to model the probability of encounter and positive catch-rate of the species of interest (Lo et al., 1992). Covariates are typically included in these delta-GLMs to account for changes in catchability (e.g. the effects of fishing gear, environmental and/or spatial differences between fishing grounds) resulting in a standardized relative abundance index (Campbell, 2004). Given that fish and fishers are not distributed homogeneously or randomly across the landscape, research developments have focused on improving delta-GLM CPUE standardization in order to produce abundance indices that are more robust to the spatiotemporal patchiness of the underlying data. This has involved either appropriately weighting spatial strata and observations in the construction of indices (Campbell, 2015) or accounting for unobserved spatiotemporal strata through imputation (Walters, 2003; Carruthers et al., 2011). Traditional delta-GLM approaches do not explicitly account for the spatial autocorrelation (spatial structure) in observations or formally incorporate imputation into the modeling process. However, the advice to impute CPUE in unsampled strata and/or to weight data based on strata area acknowledges the need to predict densities across the stock domain and weight indices based on areas (called "area weighting").

More recently, spatiotemporal methods implemented as delta-generalized linear mixed models (GLMMs) have seen greater use in fisheries-dependent CPUE standardization (Walter et al., 2014b; Thorson et al., 2015; Cao et al., 2017; Grüss et al., 2019), including in fisheries exploiting highly migratory species such as tunas (Xu et al., 2019; Ducharme-Barth and Vincent, 2020). Spatiotemporal GLMM approaches allow models to explicitly account for the spatial autocorrelation in observations and leverage the geostatistical principal that "near things are more related than distant things" (Tobler, 1970). Expanding on this idea, spatiotemporal models account for both spatial autocorrelation that is stable over time ("spatial variation") and spatial autocorrelation that changes among time steps ("spatiotemporal variation") (Thorson, 2019a). Additionally, the ability to directly incorporate imputation within the statistical model via estimated correlation structures or covariate relationships can improve predictions of density in unfished areas and help account for distributional shifts in spatial sampling (Thorson et al., 2020b).

Despite the aforementioned advantages associated with spatiotemporal models, there are additional complexities to consider relative to traditional methods of CPUE standardization. For example, spatiotemporal models are typically fit under the implicit assumption that the process for determining whether a location is sampled is statistically independent of the response at that location. When this assumption is met, then sampling location is "ignorable" and estimation can proceed as usual by specifying the probability of data conditional upon covariates and assumed model structure. However, instances when the probability of sampling is dependent upon the response at each location are called "preferential sampling" and these instances can result in biased abundance indices (Diggle et al., 2010; Conn et al., 2017; Pennino et al., 2019; Rufener et al., 2021). This bias is intuitive; for example, increased sampling in high abundance areas due to fisher targeting is assumed to cause a positive bias in observed CPUE relative to the average CPUE that would arise under random sampling (Wilberg et al., 2009).

Spatiotemporal GLMM models have also been shown to generally outperform conventional delta-GLMs and other CPUE standardization approaches in comparative simulation tests (Grüss et al., 2019; Zhou et al., 2019). However, beyond the limited fisheries-dependent simulation testing work already conducted (Grüss et al., 2019; Zhou et al., 2019), there exists a critical need to test these spatiotemporal methods in the cases where conventional geostatistical assumption of uniform or random sampling is violated (Diggle et al., 2010) such as when the spatial sampling coverage of fisheries changes over time. Furthermore, theory suggests that the bias resulting from preferential sampling will increase as a function of the variance of the residual spatial or spatiotemporal process being modeled (Conn et al., 2017). Therefore, one potential way to mitigate this bias is by including environmental covariates that can explain variation in CPUE, and thereby decrease the spatial variance of residuals. We therefore see a need to explore the potential for environmental covariates to mitigate bias resulting from preferential sampling.

The skipjack tuna (*Katsuwonus pelamis*) fishery is the largest in catch volume in the Western and Central Pacific Fisheries Commission (WCPFC) convention area (Williams et al., 2020). Historically, catches predominantly came from a broadly distributed pole-and-line fishery, of which the Japanese distant-water (*DW*) and offshore (*OS*) fleets were the primary components. In recent decades, catches from the Japanese pole-and-line (JPPL) fishery have declined and the fishery has contracted westwards across the Pacific (Kinoshita et al., 2019), and the current prevailing method of capture is via purse seine.

Standardized fisheries-dependent CPUE indices are an important input for the WCPFC skipjack tuna stock assessment (Vincent et al., 2019). Standardizing CPUE indices for the purse seine sector is challenging due to potential changes in catchability over time (Vidal et al., 2019a, 2020) and limitations in geographical scope (Vidal et al., 2019b). Given the historical distribution of the Japanese Pole-and-Line (JPPL) fishery (Ogura and Shono, 1999a) and the record of detailed change in vessel and gear configuration (Kiyofuji, 2013), the standardized CPUE index from this fishery has been used to provide relative abundance inputs for WCPFC skipjack tuna assessments (Ogura and Shono, 1999b;

Langley et al., 2010; Kiyofuji et al., 2011; Kiyofuji, 2016; Kinoshita et al., 2019). However, given the recent reduction in JPPL fishing magnitude and distribution, it is important to evaluate the further utility of this index for the WCPFC skipjack tuna stock assessment and the potential to account for this change in spatial sampling by using spatiotemporal delta-GLMMs.

The present study seeks to evaluate three questions in a simulation framework. First, it tries to understand how the nature of fisheries spatial sampling patterns may bias estimated abundance indices. Second, it seeks to determine whether shifts over time in the spatial distribution of the fishery may impact our ability to estimate temporal changes in catchability. Thirdly, it evaluates whether including a seasonal environmental covariate (sea surface temperature; SST) and/or a regional annual index (such as the Southern Oscillation Index) in the formulation of a spatiotemporal delta-GLMM can improve the estimation of abundance indices under shifts in fisheries spatial sampling. Moreover, this study applies CPUE standardization methods using a spatiotemporal delta-GLMM to a real-world application where spatial sampling has changed over time, namely the JPPL fishery for skipjack tuna in the western and central Pacific Ocean (WCPO).

2. Methods

2.1. Simulation

The simulation framework is broken into three main components: an observation model, an estimation model, and model evaluation. The observation model is described further in Section 2.1.1 which outlines how data are generated under six different spatial sampling scenarios, as well as in Section 2.1.2 which explains the two different catchability scenarios considered. The spatiotemporal delta-GLMM estimation model employed to estimate abundance indices from the simulated data is described in Section 2.1.4. A description of the metrics used to evaluate the performance of abundance indices calculated from the different combinations of observation and estimation models is provided in Section 2.1.5. Finally, two additional experiments exploring the robustness of results to assumptions in the definition of sampling scenarios are described in Section 2.1.3. The R code utilized to conduct the simulation is accessible at the following GitHub repository: https://github.com/N-DucharmeBarth/spatial.sampling.sim.manuscript.

2.1.1. Spatial sampling patterns

The simulation used a biomass field for adult skipjack from the Spatial Ecosystem and Populations Dynamics Model (SEAPODYM[1]) (Lehodey et al., 2008; Senina et al., 2020) to generate the base biomass distribution of adult skipjack tuna $S_{x,t}$ from 1979 to 2008, where x denotes a cell of 1° spatial resolution and t denotes the quarterly time step. The spatial frame of the simulation covers the spatial extent of the WCPFC stock assessment boundaries for skipjack tuna from 102° E to 210° E longitude and from 20° S to 50° N latitude (Vincent et al., 2019). SEAPODYM model output is a smooth biomass field with positive non-zero abundance predicted for all 1° spatial cells (not including land).

As fish distributions are known to be spatially patchy, areas of zero skipjack abundance were introduced. To account for this patchiness, $S_{x,t}$ was converted to a simulated biomass field $A_{x,t}$ by allowing each cell x and time t to be randomly set to zero according to a single random draw from a multinomial distribution. We treated $A_{x,t}$ as the true biomass field for simulating data and calculating performance metrics:

$$Zero \quad cells \sim Multinomial\left(1; \quad \text{size} = n_{zero}; \quad P_{zero} = \frac{1}{\sqrt{S_{x,t}}}\right) \tag{1}$$

$$A_{x,t} = \left\{ \begin{matrix} S_{x,t} \\ 0 \quad \text{if} \quad x \in \quad Zero \quad cells \end{matrix} \right\} \tag{2}$$

where n_{zero} was equal to 10% of the total number of cells-time steps ($x \times t$) in the SEAPODYM output (rounded to the nearest integer) which matched the empirical probability of non-encounter of skipjack for the JPPL fishery (Kinoshita et al., 2019); and the probability of being selected P_{zero} as a zero cell was inversely proportional to the square root of the SEAPODYM abundance ($S_{x,t}$) at location x and time t. This had the effect that cells on the fringes of the spatiotemporal distribution of skipjack tuna were more likely to have zero abundance.

To address the first question of the present study, $A_{x,t}$ was sampled under six different fishing effort patterns (one fishery-independent and five fishery-dependent) in a simulation framework based on the approach taken in Ducharme-Barth et al. (2018)). For each of the different fishing effort patterns, observation error ϵ was incorporated to produce observed (sampled) abundance $\hat{A}_{x,t}$ at each spatial cell x and time t:

$$\hat{A}_{x,t} = A_{x,t} + \epsilon \tag{3}$$

$$\epsilon \sim Normal(0, 0.15 \times A_{x,t}). \tag{4}$$

Our sampling model did not result in negative observed biomasses, because the assumed coefficient of variation was low. However, future studies that assume a higher coefficient of variation may prefer employing a positive continuous distribution (e.g. *Gamma* or *Lognormal*) to model ϵ, in order to avoid generating negative observed biomasses.

In the fishery-independent pattern (hereafter referred to as the *Random* sampling pattern), each spatial cell x had an equal probability of being selected, regardless of the underlying skipjack abundance. The five fisheries-dependent fishing effort patterns (Fig. 1) were based on the principle that fishers are more likely to fish in areas of higher abundance (Allen and McGlade, 1986; Hilborn and Walters, 1987). For both the fisheries-independent and fisheries-dependent scenarios, sampling of spatial cells within time step was done with replacement. In contrast to the *Random* sampling pattern, with the *Preferential* sampling pattern (Fig. 1 B), the probability of a spatial cell x being selected P_{pref} in any given year was proportional to simulated abundance. S_x was used, rather than A_x, in order to allow for the sampling of cells with zero abundance:

$$P_{pref,x} = \frac{(S_x)^{\phi}}{\sum (S_x)^{\phi}} \tag{5}$$

where the probability exponent ϕ controls the magnitude of preferential sampling. When $\phi = 0$ this simplifies to all spatial cells having an equal probability of being sampled (e.g. *Random* sampling) but increasing values of ϕ leads to a greater degree of preferential sampling. As a baseline for the *Preferential* sampling scenario a value of 0.5 was assumed for ϕ. This implies a weak preferential sampling where cells are selected in proportion to the $\sqrt{S_x}$, and resulted in spatial cells with higher levels of simulated abundance to have a higher likelihood of being sampled (or fished) while also allowing for sampling on the fringes of the S_x distribution. A sensitivity analysis to the choice of ϕ described in Section 2.1.3.

It is well established that perceived underlying abundance does not solely drive the distribution of fishing effort in time and space; economic

[1] SEAPODYM is an integrated age-structured, ecosystem model with explicit spatial population dynamics modeled using advective and diffusive processes. These spatial dynamics are driven by age specific environmental preference functions, based on observed environmental covariates, estimated in a data assimilation process by fitting to geo-referenced WCPFC skipjack tuna catch, size-frequency, and tag-recapture data. Senina et al. (2020)) showed that SEAPODYM is able to adequately replicate WCPO skipjack tuna dynamics including longitudinal shifts in distribution related to "El Niño" phases (Senina et al., 2008; Lehodey et al., 2020). Complete information on SEAPODYM can be found at http://www.seapodym.eu/. Details on the SEAPODYM model configuration used to produce $S_{x,t}$ can be found in Senina et al. (2018)). Please see Supplemental Information (SI) Figure 1 for a distribution of $\bar{S}_x$.

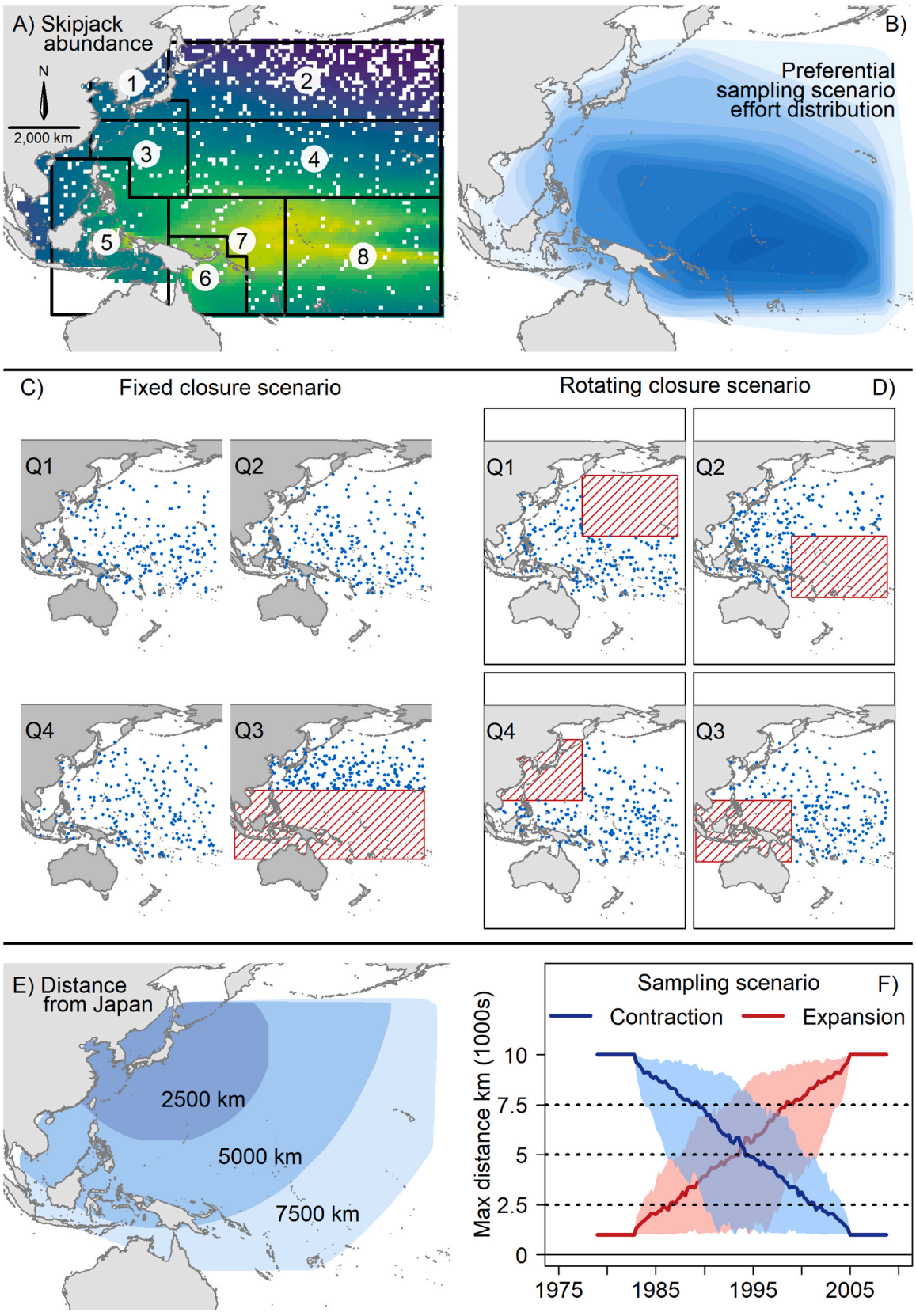

(caption on next page)

Fig. 1. A) Simulated spatial distribution of skipjack tuna (*Katsuwonus pelamis*) abundance $A_{x,t}$ in the first time period. Warmer colors indicate greater levels of abundance around the equatorial region. White pixels indicate areas of zero skipjack abundance. The eight spatial regions of the 2019 WCPFC skipjack stock assessment are shown for reference. B) Simulated snapshot of the distribution of fishing effort under the *Preferential* spatial sampling pattern. Darker, more opaque blues indicate a greater density of fishing effort. This corresponds to greater sampling in areas of higher skipjack abundance. C) Fishing effort distribution (blue pixels) under the *Fixed* spatial closure scenario, under which no fishing takes place south of 20° N in the third quarter of the year. D) Fishing effort distribution under the *Rotating* spatial closure scenario, under which quadrants of the spatial sampling frame are sequentially closed to fishing in each quarter of the year. E) Schematic indicating the approximate distances from Japan of locations within the spatial extent of the simulation. F) Maximum distance from Japan fished under the *Contraction* (blue) and *Expansion* (red) scenarios in each time step of the simulation. The solid line indicates the median maximum distance for each effort pattern across all 100 replicates while the shaded region shows the 80th-percentile across the replicates. The horizontal lines correspond to the distances depicted in the Bottom left panel.

factors and regulatory restrictions can also dictate the distribution of fishing effort (Wilen, 2004). Simplistically, a regulatory instrument such as a spatial closure can exclude fishing effort from areas that would otherwise be fished, and positive (negative) economic conditions can allow vessels to fish further away from (closer to) their home port (Holland, 2000; Smith and Wilen, 2003). Thus, an additional four fisheries-dependent sampling patterns were created, by modifying the base *Preferential* sampling pattern, to explore how these external drivers impact the ability to estimate abundance. This is by no means an exhaustive list and future work could consider the effects of other factors such as fishing tradition (Girardin et al., 2017) on spatial sampling patterns.

The two hypothetical closure scenarios were created by applying temporally varying spatial closures to the *Preferential* pattern. In the *Fixed* closure scenario (Fig. 1 C), fishing was prohibited south of 20° N during the third quarter of the year. This is similar to the current fish aggregating device fishing closure imposed on purse seine vessels targeting tropical tunas in the WCPFC convention area. Then, a second *Rotating* closure scenario (Fig. 1 D) was created by closing each quadrant of the spatial sampling frame to fishing in successive quarters of the year. The quadrants were determined by bisecting the area along the 155° E longitudinal and 15° N latitudinal axes.

Finally, hypothetical fishery *Expansion* and *Contraction* scenarios (Fig. 1 E & F) were created by applying a temporally-varying maximum distance to the distribution of fishing effort on top of the *Preferential* pattern. Japan was chosen as the "home base" for the hypothetical fishing fleet and the great-circle distance from Tokyo, Japan (139.692222° E, 35.689722° N) to every spatial cell x was calculated in kilometers using the *distHaversine* function from R package *geosphere* (Hijmans, 2019) in R 3.6.2. In the *Expansion* scenario, fishing effort was constrained to a maximum distance of 1000 km from Japan for the first 15 time steps (i.e. the first 15 quarters) of the simulation ($1/8^{th}$ of the total simulation time of 30 years or 120 quarters). Over the next 90 time-steps, the maximum distance was allowed to temporally vary according to a Brownian bridge which progressively relaxed the maximum distance to 10,000 km by the 105^{th} time-step in the simulation. All spatial cells x in the spatial sampling frame were able to be fished at this point, and this was maintained for the final 15 time steps of the simulation. The *Contraction* scenario was created in the same way but with the pattern in time-varying maximum distance reversed.

For each of the six fishing effort sampling patterns, a total of 60,000 observations were generated, and each time-step t had an equal probability of being sampled. Each combination of the six fishing effort sampling patterns and two catchability patterns (described in the following Section 2.1.2) were simulated 100 times, resulting in 1200 total data sets used to estimate abundance indices.

2.1.2. Including catchability effects

A second set of simulations was developed to address the second question of the present study, namely understanding how the changing fishing patterns impact the ability to estimate changes in catchability. This second set of simulations was identical to the six fishing effort sampling patterns described above, except that catchability effects ($Q_{v,s}$) for each vessel v and set s were incorporated into the calculation of the observed abundance or "logbook catch" records, $\hat{A}_i$. The catch record i corresponds to a discrete fishing set s by a vessel v at location x during time-step t. Under the catchability scenarios, $\hat{A}_i$ was defined as the product of simulated abundance $A_{x,t}$ and the catchability effect $Q_{v,s}$ associated with that sampling or fishing instance. Fishing effort was assumed to be equal to the unit of sampling (e.g. sets fished).

$$\hat{A}_i = A_{x,t} \times Q_{v,s} \tag{6}$$

In turn $Q_{v,s}$ was defined as the expected catchability $\overline{Q}_{v,s}$ plus a normally distributed error term.

$$Q_{v,s} = \overline{Q}_{v,s} + \epsilon \tag{7}$$

$$\epsilon \sim Normal(0, 0.15 \times \overline{Q}_{v,s}) \tag{8}$$

A normal error structure was selected as it provided a straightforward approach for linking the uncertainty in observed catch to the the expected catchability. As noted with Eq. 4, use of the *Normal* distribution could result in negative values for $Q_{v,s}$. However, given the assumed coefficient of variation this was not observed to happen. Future work using a higher coefficient of variation could consider utilizing a positive continuous probability distribution. The expected catchability for a given vessel v and fishing set s was composed of two additive ($Vessel_v$ and $Gear_v$) effects and an interactive effect ($Class_v \times Poles_{v,s}$). The rationale for the consideration of these effects is provided below. Thus, the expected catchability $\overline{Q}_{v,s}$ was expressed as:

$$\overline{Q}_{v,s} = 1 + Vessel_v + Gear_v + Class_v \times Poles_{v,s}. \tag{9}$$

Unique vessels were simulated to enter the fishery in three waves: at the start, at approximately one-third of the way through the simulation, and at approximately two-thirds of the way through the simulation. Each vessel was assumed to participate in the fishery every year up to its decommissioning age. The vessel's decommissioning age was given by a random draw from a Poisson distribution with intensity λ_a equal to one-third of the total simulation length. For each unique vessel entering the simulation, the vessel effect $Vessel_v$ was defined as a normally distributed random variable:

$$Vessel_v \sim Normal(0, 0.05), \tag{10}$$

where $Vessel_v$ was sorted such that vessels with a later start year (Y_v) in the fishery, entering the simulation in the second or third wave, had a higher vessel effect (Fig. 2 A). This simulated the subtle, intrinsic effort creep that occurs at the individual vessel level in most fisheries due to non-measurable improvements to technical efficiency (Eigaard et al., 2014).

In the case study, vessels operating in the Japanese pole-and-line fishery for skipjack either belong to the *OS* class or the *DW* class. *DW* vessels are larger ($\geq$ 200 gross registered tons; GRT) allowing them to fish more poles; and to fish further from Japan. They also have recorded information on gear configuration such as bird radar, sonar, and bait tanks. For the purposes of the simulation the vessel class effect $Class_v$, *OS* or *DW*, assigned to each simulated vessel upon entrance into the fishery was based on the results of a single Bernoulli draw with equal probability of success.

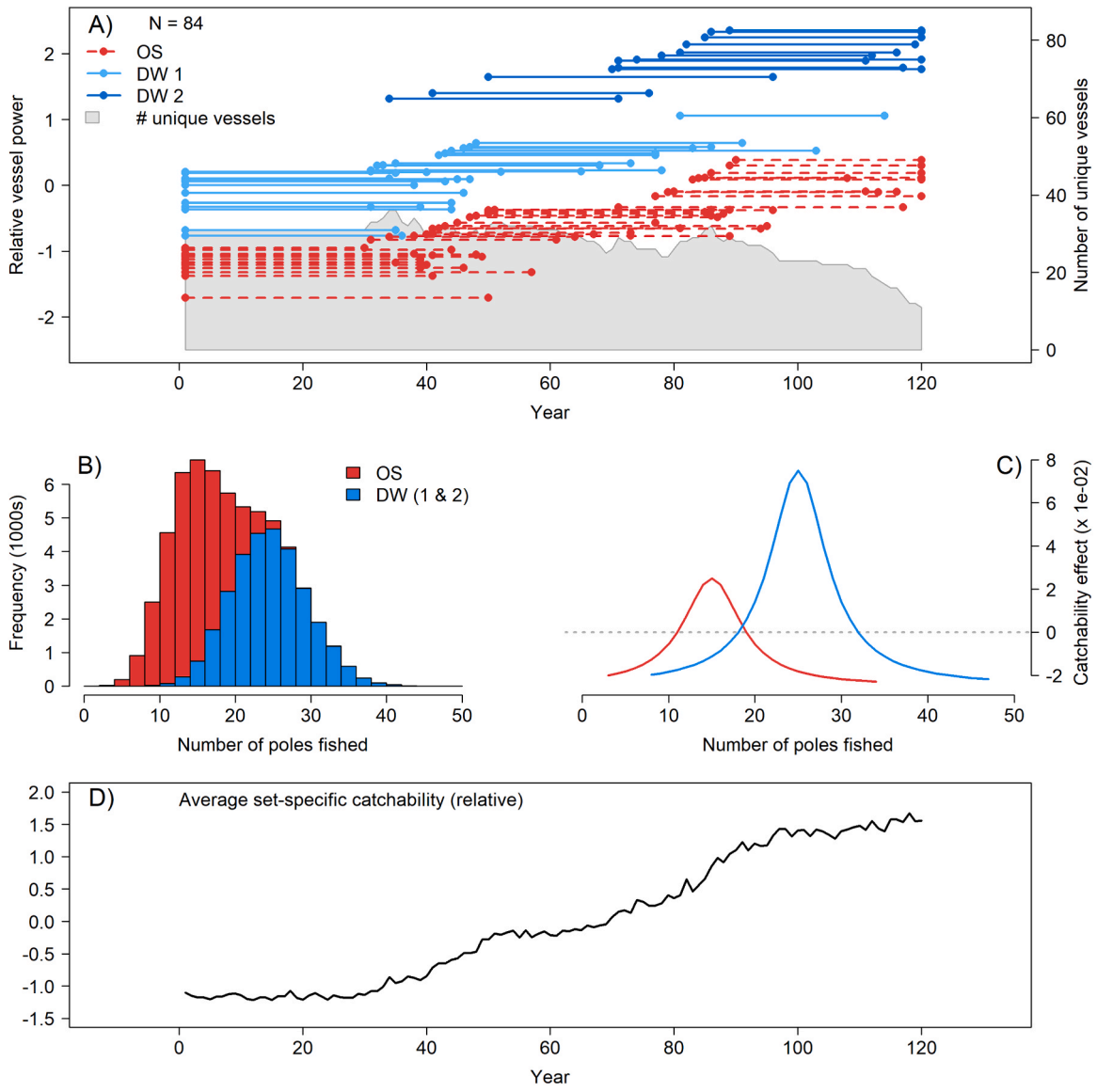

Fig. 2. Top: Example of simulated fleet composition over time. Red dotted lines indicate offshore (*OS*) vessels and blue solid lines indicate distant water (*DW*) vessels. Dark blue indicates a *DW 2* vessel with a higher catchability effect. The start and end of each line indicates the activity period for unique vessels. The left y-axis indicates the relative vessel power of each vessel (as a combination of $Vessel_v$, $Gear_v$, and $Class_v$) where vessels entering the simulation at a later year have a higher relative vessel power compared to others in the same class. The gray polygon gives the number of unique vessels active in the fishery over time. Middle left: The cumulative distribution of the number of poles fished with the color indicating the corresponding vessel class, *OS* (red) and *DW* (blue). Middle right: The interactive effect on catchability of vessel class and number of poles fished. Bottom: Average set-specific catchability $\overline{Q}_{y,s}$, on a relative scale, over time.

$$Class_v = \left\{ \begin{array}{ll} \text{DW} & \text{if} \quad Bernoulli(1, p = 0.5) = 1 \\ \text{OS} & \text{if} \quad Bernoulli(1, p = 0.5) = 0 \end{array} \right\} \tag{11}$$

Each unique vessel entering the fishery was determined to have a gear effect $Gear_v$ that was based in part on the vessel's class designation (*DW* or *OS*) and the vessel start year Y_v. Depending on the year entered, a *DW* vessel was randomly assigned either a lower (*DW 1*) or higher (*DW 2*) gear effect. In this simulation the gear effect was viewed as a proxy variable to represent increases in catchability due to the large scale adoption of improved fishing technologies (gear configuration) at the fleet level as they became available. In the case of the Japanese pole-and-line fishery these changes to gear configuration included the adoption of improved bird radars to aide in the discovery of surface schools (~ 1987), low-temperature bait tanks which improved the survival of bait fish used to encourage feeding around the vessel (~ 1982), and sonar to locate schools (~ 1982) (Shono and Ogura, 2000; Kiyofuji, 2013). *DW* vessels entering the fishery later in the simulation period had a better chance of being assigned a "better" gear configuration and had a higher $Gear_v$ effect to reflect this.

$$Gear_v = \left\{ \begin{array}{c} 0.1 \times Binomial(1, \frac{1}{1+exp(-0.12 \times (Y_v - 60))}) \text{ if } Class_v = \text{DW} \\ -0.05 \text{ if } Class_v = \text{OS} \end{array} \right\} \tag{12}$$

Lastly, given the difference in size between the two vessel classes, an interaction between the number of poles fished and the vessel class was considered. For each set s fished by a vessel, the number of poles fished p_s was given as a random draw from the Poisson distribution with intensity λ_p specified by the vessel class (Fig. 2 B). A quadratic effect on catchability with respect to the number of poles fished was included, $Poles_{v,s}$ (Fig. 2 C). The rationale behind this modeling choice is that, up to a certain point, more poles results in a greater catchability, yet too many poles can result in reduced catchability due to over-crowding:

$$Poles_{v,s} = \left\{ \begin{array}{ll} 0.10 \times (0.75 + \frac{-(0.25 \times p_s - 6.25)^2}{1 + (0.25 \times p_s - 6.25)^2}) & \text{if} \quad Class_v = \text{DW} \\ 0.05 \times (0.50 + \frac{-(0.25 \times p_s - 3.75)^2}{1 + (0.25 \times p_s - 3.75)^2}) & \text{if} \quad Class_v = \text{OS} \end{array} \right\} \tag{13}$$

$$p_s \sim \left\{ \begin{array}{ll} Poisson(\lambda_p = 25) & \text{if} \quad Class_v = \text{DW} \\ Poisson(\lambda_p = 15) & \text{if} \quad Class_v = \text{OS} \end{array} \right\} \tag{14}$$

An example of the simulated fleet and vessel characteristics across time is shown in Fig. 2 A & D.

2.1.3. Sampling sensitivity

The spatial sampling scenarios described in Section 2.1.1 made specific assumptions as to the degree of spatial change in sampling distribution (*Expansion/Contraction* scenarios), and also the strength of the probability weight used to define the *Preferential* sampling. In order to ascertain the robustness of results to these specific assumptions, two additional simulation experiments were developed.

In order to further evaluate the effects of fishing distribution contraction on the ability to recover the true population trend, additional data-sets were simulated under the *Contraction* sampling pattern described in Section 2.1.1 where the degree of spatial contraction was controlled. Eight "sets" of 10 replicates of data (80 total data-sets) were simulated where each "set" of data had a progressively greater maximum distance from Japan (in increments of ~ 1, 285 km from 1000 km up to 10,000 km) in the final 15 time-steps of the simulation (SI Figure 5). Each data-set assumed vessels could fish up to a maximum distance of 10,000 km in the initial 15 time-steps of the simulation. Additionally, each of the 80 data-sets were modeled with and without catchability effects (see Section 2.1.2 for a description of the catchability effects). This sensitivity experiment allowed us to gauge how model performance degraded as a function of a reduction in the area sampled by exploring an additional range of sampling scenarios book-ended by the *Contraction* sampling pattern at one extreme and the *Preferential* sampling pattern at the other.

A similar experiment was devised to evaluate the potential bias and error caused by varying strengths of preferential sampling. Eight "sets" of 10 replicates of data (80 total data-sets) were simulated where each "set" of data had a greater probability weight ϕ used to define the strength of the preferential sampling ($\phi \in \{0, 0.25, \mathbf{0.5}, 1, 1.5, 2, 4, 8\}$). The value in bold ($\phi = 0.5$) indicates the assumption of weak preferential sampling made in the *Preferential* sampling pattern, while a value of zero for ϕ would produce samples equivalent to the *Random* sampling pattern. The average spatial distribution of sampling effort for various values of the probability exponent ϕ are shown in SI Figure 6. Similarly to the *Contraction* sensitivity, each of the 80 data-sets were modeled with and without catchability effects.

2.1.4. Estimating indices

For each of the 1200 simulated data sets described in Section 2.1.1, four different configurations of a spatiotemporal delta-lognormal GLMM implemented using R package *VAST* release number 3.2.2[2](Thorson, 2019a) were employed to estimate abundance indices I_t from the simulated logbook data $\hat{A}_i$. A baseline configuration of the spatiotemporal model[3] consisted of specifying two sub-models, as in any delta model: one for modeling the encounter probability with a binomial error structure, and one for modeling positive catch component with a lognormal error structure (Lo et al., 1992). Each sub-model separately estimated spatial variation (spatial random effects) as well as spatiotemporal variation (a set of spatiotemporal random effects for each unique combination of spatial time-step) at 150 "knots" that were uniformly distributed across a 1° spatial extrapolation grid defined by the model's spatial domain. In this case the model spatial domain was defined as a convex hull around the observed sampling locations with a ~ 275 km buffer. The spatial correlation structure of both the spatial random effects and the spatiotemporal random effects was governed by a multivariate normal random field with a Matérn spatial covariance function. For the spatiotemporal random effects, no correlation structure was assumed for the temporal component of variation. Indices were calculated as a spatial average of the predicted density across the model extrapolation grid. Uncertainty around the index was derived using a generalization of the delta-method (Kass and Steffey, 1989). Though the results focus on the index estimated for the entire WCPFC assessment area, abundance indices were simultaneously estimated by a spatiotemporal model for the eight regions within the assessment area (Fig. 1 A).

In order to examine the effect of changing the spatiotemporal model structure on the estimated indices, four alternative configurations of the spatiotemporal model were developed. Model configuration was done according to a full factorial combination of either including a seasonal environmental covariate on abundance (SST) or including a regional annual climate index (the Niño 4 index) as a spatially varying coefficient (SVC; Thorson, 2019b). This resulted in the following four configurations: the baseline spatiotemporal model described above (*NoE*), the baseline spatiotemporal model with the inclusion of an environmental covariate (*E*), the *NoE* spatiotemporal model with the inclusion of a regional annual climate index as a SVC (*NoESVC*), and the *E* spatiotemporal model with the inclusion of a regional annual climate index as a SVC (*ESVC*). Model selection (using Akaike's Information Criteria or otherwise) was not explicitly addressed in this study. However information on relative model performance (and therefore selection) is available in the Supplemental Information section "Model selection". Future studies could more explicitly explore the consequences of conducting model selection among covariates on spatiotemporal CPUE standardization performance (e.g. Han et al., 2021).

For the *E* and *ESVC* models, the Reynolds monthly 2° gridded SST data[4] (Smith and Reynolds, 1981) from 1979 to 2008 aggregated to a quarterly time scale was included as a covariate using a three-degree polynomial spline implemented using the bs function in R package *splines* (R Core Team, 2021). Skipjack tuna are most abundant in tropical waters so it is expected that SST and skipjack abundance are positively correlated (See SI Figure 2). Implementing the relationship as a polynomial spline allows for the estimation of an optimal temperature with estimated abundance declining as the temperature moves away from the optimum. Additionally note that, within the SEAPODYM model, a temperature preference for adult skipjack tuna is estimated and used as a component of the advective movement of adult skipjack biomass in the model (Senina et al., 2020).

In the *NoESVC* and *ESVC* models, the quarterly Niño 4[5] index was included as a SVC. Skipjack tuna are known to shift their distribution towards the central Pacific during negative or "El Niño" phases of the Southern Oscillation Index (Lehodey et al., 1997) which has been replicated using SEAPODYM (Senina et al., 2008; Lehodey et al., 2020). The Niño 4 index is the western most Niño index, and is the temperature anomaly calculated over a region (160° E to 210° E longitude and from 5° S to 5° N latitude) which overlaps the most with the spatial simulation frame. For reference, positive temperature anomalies in the Niño 4, hereafter referred to as ENSO, box coincide with "El Niño" conditions or negative phases of the Southern Oscillation Index. Including the climate

[2] Accompanying utility functions for *VAST* used in this analysis can be found in v1.0.0 of the R package *ofp-sam-vast-utils*: https://github.com/PacificCommunity/ofp-sam-vast-utils/releases/tag/v1.0.0

[3] A technical description of the spatiotemporal model can be found in the Supplemental Information section "*VAST* Technical Annex".

[4] https://podaac.jpl.nasa.gov/dataset/REYNOLDS_NCDC_L4_MONTHLY_V5

[5] https://psl.noaa.gov/enso/dashboard.html

index as an SVC in the spatiotemporal model results in the estimation of an additional set of mean zero random effects (corresponding to the aforementioned "knots"), and an extra fixed effect (the random effect variance term) for each component of the delta model. These extra random effects can be interpreted as the slope of the relationship between abundance at that spatial location and the ENSO index. A positive random effect indicates that abundance is estimated to increase at that given location with "El Niño" phases of the climate index, and the magnitude of the random effect will give the size of the estimated change in abundance (Thorson, 2019b). Additional detail on how environmental covariates are included in the VAST model is provided in Supplemental Information section "*VAST* Technical Annex".

For the data sets where catchability effects were included, the four spatiotemporal model configurations were modified to include the estimation of normally distributed vessel random effects RE_v and the estimation of fixed effects for the remaining catchability components $\hat{Q}_i$ for both the binomial and lognormal components of the model. These models are indicated by the prefix *Q-* and additional detail on the construction of these models is provided in Supplemental Information section "*VAST* Technical Annex".

$$RE_v \sim Normal(0, \sigma_v) \tag{15}$$

$$\hat{Q}_i \sim Gear_i + Class_i \times bs(Poles_i, \quad df = 3) \tag{16}$$

Lastly, for the purposes of the two additional sampling sensitivity experiments described in Section 2.1.3, *Contraction* and *Preferential*, only the *NoE* and *Q-NoE* model formulations were considered.

2.1.5. Model Performance

Model performance in all simulations was evaluated relative to the "true" index from the SEAPODYM output, T_t. Regional indices were calculated by summing up all $A_{x,t}$ within each time step for the cells x that fell within the boundaries of the given region.

$$T_{r,t} = \sum_{x=1}^{n_x} A_{x,t} : x \in Region_r \tag{17}$$

The estimated index I_t is calculated at each time step within VAST as the sum of the area $\times$ predicted density across all grid cells defined within the model domain. Prior to assessing model performance, all indices (estimated I_t and true T_t) were rescaled to a mean of 1 by dividing by the overall index mean. Model performance was assessed in three different ways: error, bias, and coverage.

Model error was measured using root mean squared error (RMSE; Stow et al., 2009):

$$RMSE = \sqrt{\frac{\sum_{t=1}^{n}(I_t - T_t)^2}{n}}. \tag{18}$$

A model with no error would have an RMSE of 0. Additionally, RMSE gives greater weight to larger errors (as compared to mean absolute error) so poor fits to the true index are penalized and result in a larger RMSE (Stow et al., 2009).

Model bias was measured as the slope parameter β from a linear model between the true index T_t and the simulated index I_t (Thorson et al., 2015; Grüss et al., 2019):

$$I_t = \alpha + \beta \times T_t + \epsilon_t \tag{19}$$

$$\epsilon_t \sim Normal(0, \sigma_\epsilon^2). \tag{20}$$

A β of 1 indicates that the estimated index accurately tracks changes in the true index. A β greater than 1 indicates that the estimated index I_t overestimates the true change in abundance over time, while a β less than 1 indicates that the estimated index I_t underestimates the true rate of change of abundance (Wilberg et al., 2009; Thorson et al., 2015).

Finally, coverage was calculated (Equations 21 & 22) as the proportion of years over the study period that the estimated 50% confidence interval contained the true index (Agresti and Coull, 1998; Newcombe, 1998; Brown et al., 2001):

$$Coverage = \frac{1}{t}\sum_{t=1}^{n} C_t \tag{21}$$

$$C_t = \left\{ \begin{array}{l} \text{if} \quad T_t \le I_t + Z_{50\%}\sigma_{I_t} \quad \text{and} \quad T_t \ge I_t - Z_{50\%}\sigma_{I_t} \quad \text{then} \quad C_t = 1 \\ \text{else} \quad C_t = 0 \end{array} \right\} \tag{22}$$

where $Z_{50\%}$ is the Z-score associated with the 50% confidence interval (0.675) and σ_{I_t} is the time varying model-estimated uncertainty around the estimated index I_t, defined as a standard error. Well-performing confidence intervals are ones where the nominal (predetermined) probability equals the actual proportion of years where the confidence interval contains the true value. Assuming the estimated index is approximately unbiased and that the predetermined probability is 50%, the target level of *Coverage* is 0.5. *Coverage* values greater than 0.5 indicate that the estimated confidence intervals are too wide and *Coverage* values less than 0.5 indicate that the estimated confidence intervals are too narrow (Bolker, 2008; Johnson et al., 2016). *Coverage* values of less than 0.5 could also be an indication that there is bias in the estimated index and that the estimation model is unable to capture the true value. Coverage metrics can of course be calculated for any level of confidence interval, though the inference drawn will be the same. For completeness, additional coverage metrics were calculated for the 70% and 95% confidence intervals and these can be found in Supplemental Information section "Additional coverage metrics".

We determined if the spatiotemporal models were converged by checking that the gradient of the marginal log-likelihood was less than 0.0001 for all fixed effects, and that the Hessian matrix of second derivatives of the negative log-likelihood was positive definite. Spatiotemporal models that did not meet these criteria were excluded from analyses. Additionally, spatiotemporal delta-GLMMs are computationally intensive and a subset of models failed to estimate for computational reasons (e.g. running out of available memory on the compute machine), and these models were also excluded from the analysis.

2.2. Fishery application

2.2.1. Description

Spatiotemporal delta-GLMMs were also applied to the analysis of catch records from a fishery where the spatial sampling has changed over time, in this case the JPPL fishery for skipjack tuna in the WCPO (Fig. 3). Daily catch observations from the JPPL fishery, where catch was recorded as metric tons (mt) of skipjack tuna caught per day, were available for the period of 1972–2018 from the National Research Institute of Far Seas Fisheries (NRIFSF) operational logbook. This corresponded to 1,088,659 daily catch records. Data were collected with a 1° spatial resolution, where the position recorded in the logbook was the noon position from that day's fishing activities. In addition to the catch, date and location of fishing activity; the logbook records also contained detailed information about the vessel including vessel class (*OS* or *DW*), GRT (vessel size), vessel identifier, the average number of poles fished that day, and in the case of DW vessels, the gear configuration/fishing technology employed (i.e. presence of low temperature live bait tank, type of bird radar, sonar, NOAA meteorological satellite image receiver; see Shono and Ogura, 2000 for more information).

Preparation of the data for the current analysis followed the "SP2″ data-screening procedure for the "geostatistical delta-GLMM" analysis conducted in support of the 2019 WCPFC skipjack tuna stock assessment (Vincent et al., 2019) as described in Kinoshita et al. (2019)). Briefly, this screening process 1) removed data from vessels that had operated for less than five years and less than 10 days per year, 2) removed vessels that did not have any vessel ID information, 3) removed *DW* vessels

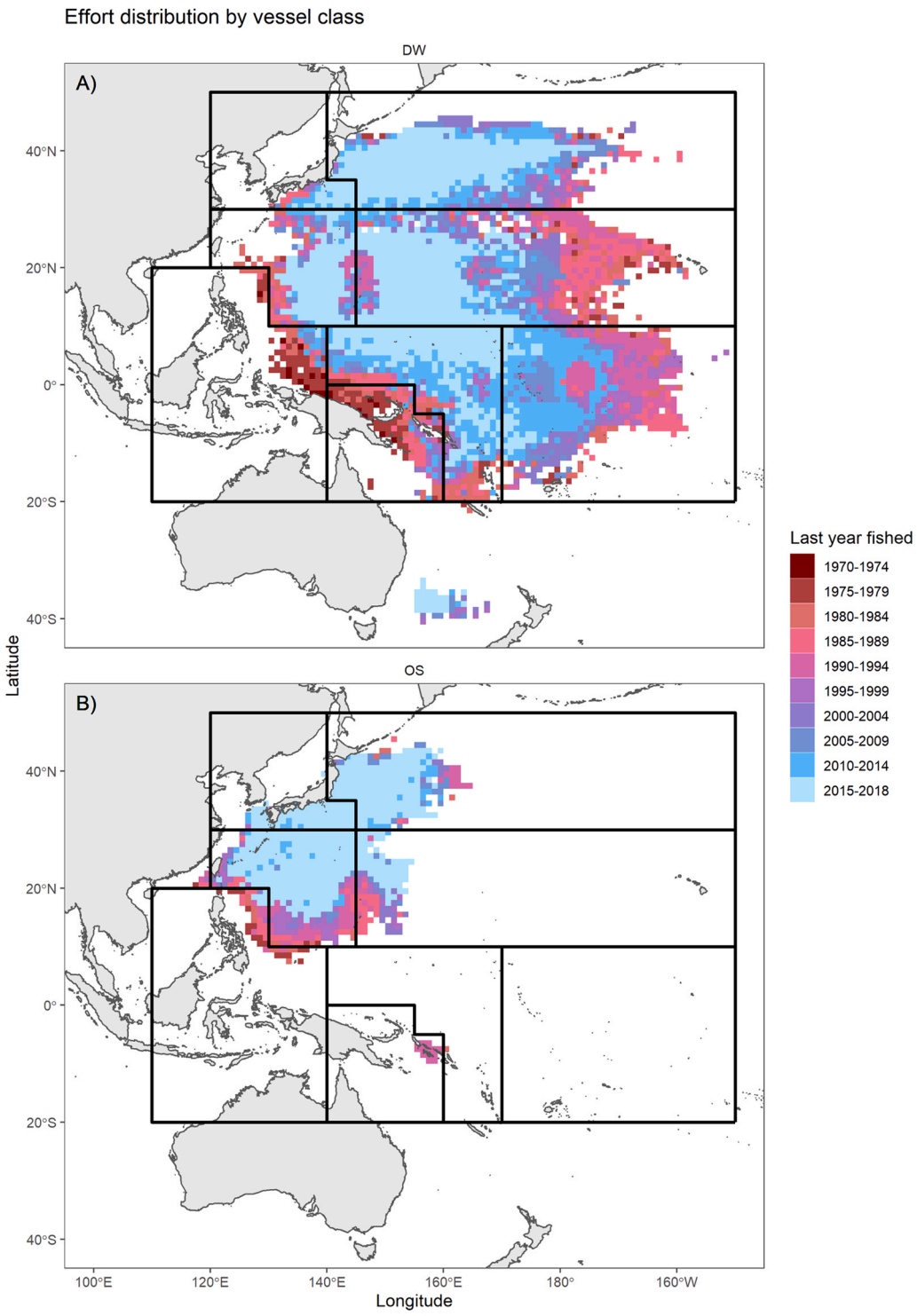

Fig. 3. Spatial distribution of the Japanese pole-and-line (JPPL) fishery by vessel class: distant-water (*DW*; top) and offshore (*OS*; bottom). The color of the 1˚ spatial cell indicates the last year that a vessel fished in that cell. The 2019 WCPFC stock assessment boundaries are superimposed on the distributions of fishing effort (black lines). *Note: A confidentiality mask has been applied such that 1˚ spatial cells plotted in the figure correspond to data from at least three unique vessels.*

without gear configuration information, and 4) removed data with unlikely values; namely fewer than two poles fished, fewer than five crew members, and catches greater than 200 mt.

2.2.2. *Estimating indices*

The spatiotemporal delta-GLMM models used to estimate indices from the JPPL operational data were structured following the models described in Section 2.1.4, while also incorporating knowledge from previous spatiotemporal delta-GLMM modeling of this data set (Kinoshita et al., 2019). The four configurations of the spatiotemporal model including catchability effects described in Section 2.1.4 were constructed: *NoE*, *E*, *NoESVC*, and *ESVC*. However, instead of modeling the relationship with SST using a cubic-spline, a simpler linear relationship was assumed as in Kinoshita et al. (2019)). Preliminary models from Kinoshita et al. (2019)) where SST was modeled using a cubic-spline showed a counter intuitive result in the estimated SST

relationship with peak skipjack catch-rates occurring in cooler waters. This was hypothesized to occur due to high catch-rates fishing near temperature fronts in the warm, Kuroshio Extension current (140°E to 170°E & 30°N to 50°N) and a mismatch in the resolution of the associated environmental covariate. A sensitivity model (*E.Spline*) where the SST relationship was modeled with a cubic-spline was estimated for comparison.

The modeling of catchability effects also varied slightly from the approach described in Section 2.1.4. Following Kinoshita et al. (2019)) the models for the fishery application estimated a normally distributed vessel random effect and accounted for vessel class, vessel size and number of poles fished as catchability components $\hat{Q}_i$ as follows:

$$\hat{Q}_i \sim Class_i + bs(Poles_i, \quad df = 5) + bs(GRT_i, \quad df = 5) \tag{23}$$

Information on gear configuration/fishing technology was not accounted for in the standardization model as this information was unavailable for the *OS* component of the fishery. However, preliminary models fit solely to *DW* trips, where this information was available, showed that including these covariates resulted in negligible change to the estimated index.

Though the same data and data-preparation methods were employed as in Kinoshita et al. (2019)), there are some differences in the models used for index standardization that preclude the direct comparison with the indices used in the 2019 WCPO skipjack tuna stock assessment (Vincent et al., 2019). In addition to the aforementioned differences, the current analysis is based on a spatiotemporal model structure with 150 uniformly distributed spatial "knots" or random effects whereas the indices developed in Kinoshita et al. (2019)) were based on 288 spatial "knots" that were distributed in proportion to the spatial density of the data. Furthermore, the spatiotemporal delta-GLMM used in Kinoshita et al. (2019)) modified the *VAST* source code to apply a temporal-mask in the calculation of the standardized indices from the abundance estimated at all extrapolation grid cells. This mask functioned such that the predicted abundance from cells which were deemed to be "biologically unfeasible" did not factor into the spatial average to generate the estimated abundance index. In the case of the Kinoshita et al. (2019)) analysis, cells were excluded from the calculation if their average temperature was below a minimum temperature threshold (18°C for skipjack; Kiyofuji et al., 2019) for the time-step in question.

3. Results

3.1. Simulation

Relative to the nominal CPUE trends, spatiotemporal models appear to be able to better account for shifts in fisheries spatial sampling and produce abundance indices that more closely reflect the "true" abundance trend at the level of the entire WCPO region (Fig. 4). However, estimation model performance was not consistent across the spatial sampling patterns considered. Unsurprisingly, the *Random* and *Preferential* spatial sampling patterns produced abundance indices that were approximately unbiased (under both the catchability and no catchability scenarios; Fig. 5 G & H), with the lowest level of error (Fig. 5 A & B), and confidence intervals with the appropriate level of coverage (Fig. 5 M & N). However, an unexpected result was that estimated abundance indices from the *Preferential* sampling pattern appeared to be qualitatively less biased than abundance indices from the *Random* effort pattern (Fig. 5 G & H), though there was considerable overlap in the degree of bias measured from models under both spatial sampling patterns. This finding was more thoroughly explored in a sensitivity experiment (Section 3.1.1). Spatiotemporal models also appeared to perform fairly well under the *Rotating* seasonal closure scenario (Fig. 5 F, L & R). Furthermore, under the *Rotating* seasonal closures scenario, when variable catchability was introduced, abundance indices appeared qualitatively less biased than abundance indices estimated from either the *Preferential* or *Random* spatial sampling patterns (Fig. 5 L). By comparison, performance of spatiotemporal models estimated from the *Fixed*

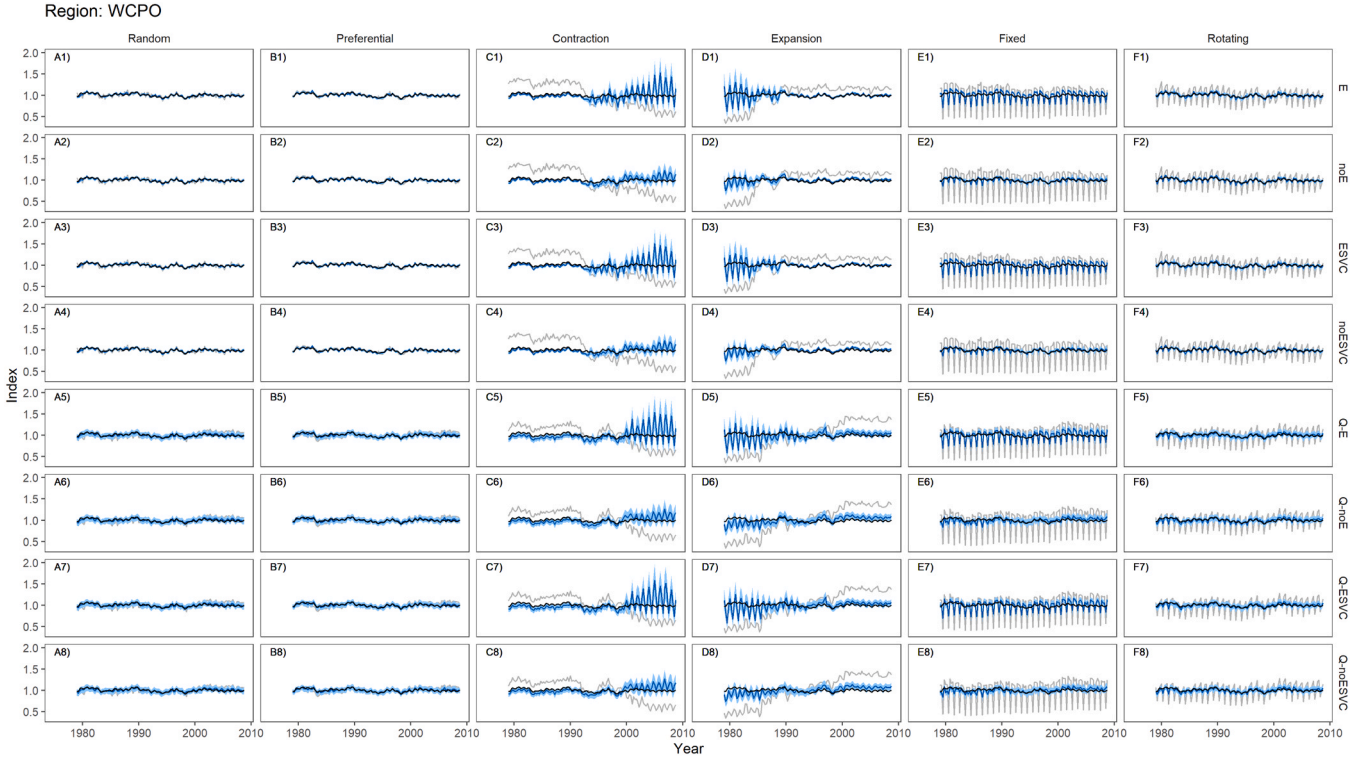

Fig. 4. Example time series from a single replicate of each of the 42 spatial sampling scenario (columns) and estimation model (rows) combinations. In each panel the "true" simulated index is shown by the bold black line, the nominal unstandardized index is shown with the thin gray line, and the standardized index is shown in blue with the 95% confidence interval denoted by the shaded polygon. All indices were normalized to a mean of one for plotting.

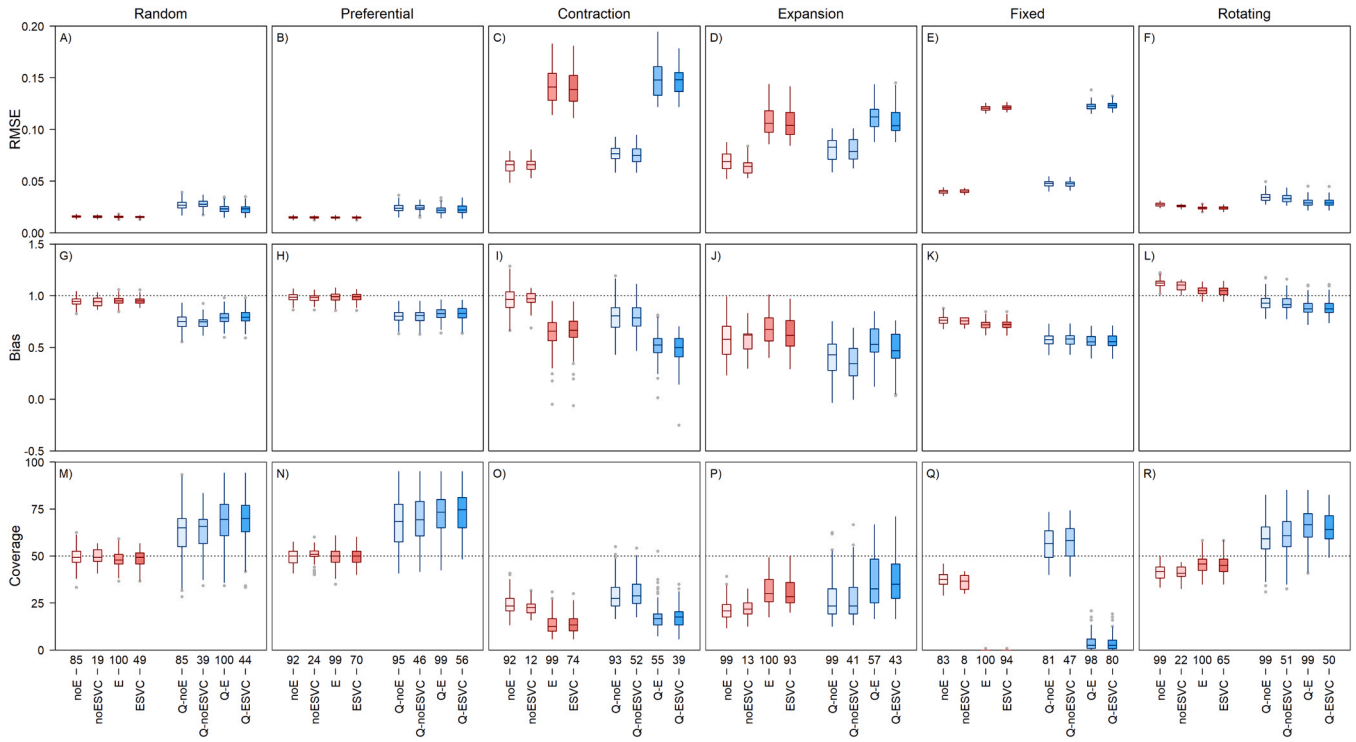

Fig. 5. Summary of the three metrics (rows) calculated across all replicates for each of the 42 spatial sampling scenario (columns) and estimation model (x-axis within each panel) combinations. The three metrics include: root mean squared error (RMSE), bias, and confidence interval coverage (see Section 2.1.5 for a description of the metrics). Each panel contains box plots showing the 25^{th} percentile, median, and 75^{th} percentile across all retained replicates. Outlier replicates are shown as gray points and these were determined as being more than 1.5 times outside of the inter-quartile range. The blue boxplots correspond to models where catchability effects were simulated and estimated, while the red box plots correspond to models where catchability effects were not simulated and not estimated. The number of replicates meeting the criteria for retention in the analysis is listed above the name of the model at the bottom of the figure.

seasonal closure scenario was dragged down by poor estimation in the closure quarter, particularly when SST was included as an environmental covariate (Fig. 4 E2 & E4). Abundance indices from the *Expansion* and *Contraction* scenarios were also quite poorly estimated and tended to underestimate the true rate of change in the simulated abundance trends ($\beta < 1$; Fig. 5 I & J). This was not unexpected given the extreme shifts in sampling distribution simulated under both of these scenarios. Additionally, the abundance indices from the *Expansion* and *Contraction* scenarios grew quite variable when sampling effort was constrained to the area around Japan. This is also expected, as seasonal variation in abundance, in the real world but also in SEAPODYM, is highest in the northern latitudes around Japan. This particular result may not be completely generalizable to cases where the degree of seasonal variability is perhaps more homogeneous across the sampling and model domains.

In general, the models from scenarios where catchability effects were simulated and estimated produced abundance indices with similar levels of error as the models from scenarios where catchability effects were not simulated and not estimated (Fig. 5 A-F). However, the models where catchability was estimated tended to produce abundance indices with a greater degree of bias and wider confidence intervals relative to the indices from scenarios without catchability effects simulated. This marginally worse performance is expected given that the spatiotemporal models are estimating additional catchability-related fixed and random effects from the same quantity of input data. It is encouraging that despite this, the models do appear to be able to disentangle temporal changes in catchability from temporal changes in the sampled population (due to natural variability and shifts in spatial sampling), provided the shifts in spatial sampling are not too extreme. However, it is worth noting that the catchability models tested in our simulation framework were specified to match the operating model under which the catchability effects were generated. These results may not hold in cases where the estimation model is mis-specified (i.e. where missing catchability variables are non-random with respect to spatial location or other model components).

Under spatial sampling scenarios with a good spatiotemporal sampling coverage (i.e. under the *Preferential* and *Random* scenarios), the inclusion of an environmental covariate on abundance (SST) or an SVC (ENSO index) in the spatiotemporal model did not meaningfully alter the estimated abundance indices at the level of the entire WCPO region. The effect of including the SST as a covariate was mixed for scenarios with impaired spatiotemporal coverage (i.e the four other sampling scenarios considered in this study), though inclusion of the ENSO index ($-$ *SVC* models) still did not have a noticeable influence on the estimated abundance indices. Under the *Rotating* closure scenario, including the environmental covariate reduced error (Fig. 5 F & L) and bias, while resulting in a more appropriate confidence interval coverage under the no catchability scenario. This pattern reversed once catchability effects were simulated and estimated. For the *Fixed* spatial closure scenario, including the environmental abundance covariate substantially degraded model performance and coverage levels, as the estimated SST relationship with abundance was biased by the exclusion of observations from the WCPO "warm-pool" in the third quarter of the year. Though inclusion of SST resulted in greater error under the *Expansion* and *Contraction* scenarios, it did appear to improve confidence interval coverage and measured bias for the *Expansion* scenario (Fig. 5 J & P).

A total of 4800 estimated indices were considered in this analysis. Application of the retention criteria based on model convergence and completion retained 3339 models ($\sim$ 70%). We note that models where SVC was included tended to fail at a higher rate resulting in the fewest retained replicates. This is likely due to poor estimation of the associated random effects resulting in a singularity issue during model estimation.

3.1.1. Sampling sensitivity

As expected, abundance index performance degraded as a function of decreasing spatial extent of sampling. This was most apparent in terms of model error (Fig. 6a), while both bias (Fig. 6b) and confidence interval coverage (Fig. 6c) degraded more slowly. In general, abundance index performance did not meaningfully degrade until the proportion of the area sampled in the final time-steps fell below 20–40% of a given region. At the scale of the entire WCPO region, this occurred once the simulated fishing fleet had contracted to within 3600 km from Japan in the final time-steps, but at a distance of 6200 km in the context of assessment region 8 (See Fig. 1 A for map of assessment regions). Metrics within the assessment region closest to the Japanese mainland (i.e. region 1), were essentially unchanged as simulated fishing contracted, and even marginally improved as sampling became increasingly concentrated in the region.

An encouraging sign was that abundance index performance appeared to be similar between scenarios where catchability effects were simulated and estimated and scenarios where they were not. This indicated that shifts in spatial sampling did not completely compromise the model's ability to correctly estimate potentially confounded temporal shifts in catchability. However, when catchability effects were estimated, there was some indication that there was a slight underestimate of the true rate of change in the abundance index relative to when catchability effects were not simulated/estimated (Fig. 6b 1–3). Additionally, confidence intervals were estimated to be too broad in the abundance indices from scenarios where catchability were estimated (Fig. 6c 1–3).

Further investigation into the aforementioned finding that abundance indices estimated from the *Preferential* sampling scenario showed equal or better performance than those abundance indices estimated from the *Random* spatial sampling pattern indicated that this was not a robust finding and was dependent on the intensity of simulated preferential sampling. As expected, when spatial sampling contracted into the core of the simulated skipjack distribution due to high preferential sampling intensity ($\phi \gg$) model error increased (Fig. 7a), the estimated abundance index no longer changed at a rate proportional to simulated abundance (Fig. 7b), and estimated confidence tended to be overly tight (Fig. 7c). However, degradation in estimated abundance index performance was not linearly related to ϕ. Abundance indices estimated from spatial sampling scenarios where simulated with ϕ less than 1, performed similarly and in fact optimal metrics were achieved when ϕ fell within a range of 0.5–2. Inference was similar between scenarios where catchability effects were simulated and estimated and scenarios where they were not, though scenarios where catchability effects were simulated and estimated showed relatively worse performance.

3.2. Fisheries application

Skipjack tuna relative abundance indices for the JPPL fishery in the WCPO were virtually identical across the four candidate models and the sensitivity model. Given this similarity, presentation of the results will focus on the ESVC model (An Akaike Information Criterion table for the models can be found in Supplemental Information section "Model selection", and model outputs for the ESVC model can be found in Supplemental Information section "VAST outputs"). Despite accounting for vessel ID, vessel class, vessel size, and number of poles fished, the estimated abundance index was largely consistent with the nominal CPUE and showed a largely flat trend across the model period (Fig. 8). Model regions 5 and 6, which exhibited the poorest spatial sampling over the model period, showed the largest deviation from the nominal CPUE. The absence of observations meant that the abundance indices estimated in model regions 5 and 6 were mostly driven by patterns in predicted abundance from adjacent regions via the spatial correlation structure estimated by the spatiotemporal model. Seasonal variability was evident in all model regions, though the most temperate model regions (i.e. regions 1 and 2) showed the greatest degree of intraannual variation.

Inference about the relationship between SST and skipjack positive catch-rate (or encounter probability) could change as a result of the functional form used even if this does not translate to a perceptible difference in the estimated relative abundance index (Fig. 9). Given that skipjack is a tropical tuna species with the bulk of the biomass distribution located within 10° latitude of the equator (Moore et al., 2020), it is unsurprising that both the linear effect (*E & ESVC*) and the cubic spline (*E.Spline*) formulations estimated a positive relationship between SST and encounter probability for WCPO skipjack. Surprisingly, the *E.Spline* model estimated a quasi-parabolic relationship between SST and positive catch-rates, with catch-rates predicted to be lower in temperate waters, and high in waters below 18° C (which is the lower thermal limit for skipjack; Kiyofuji et al., 2019). This estimated relationship is likely driven by high reported catch-rates from JPPL vessels fishing in the Kuroshio Extension area during the first and fourth quarters of the year, and the potential for skipjack tuna to make very brief forays into colder waters below the thermal limit, as identified in archival tagging data (Kiyofuji et al., 2019).

Estimated skipjack spatial distribution patterns from JPPL fisheries data corroborate our existing understanding of the WCPO skipjack stock's spatial and temporal dynamics (Fig. 10). As described in Moore et al. (2020)), encounter-rates are predicted to be highest within tropical and sub-tropical waters in the WCPO (~ 30°S to 30°N latitude), with catch-rates higher in the equatorial (10°S to 10°N latitude) central Pacific Ocean. As seen in Fig. 10 (top-right), the *ESVC* model also estimates very high catches off of south-eastern Australia where the East Australian Current splits off from the coast to form the Tasman Front. This is likely a data artifact given the very small number of observations from this area (all within recent years). However, oceanographically this area is similar to the Kuroshio extension area where a warm-water current meets a cold-water mass.

4. Discussion

Consistent with previous observation and research (Carruthers et al., 2010; Maunder et al., 2020), this paper explicitly demonstrates how common fisheries-dependent sampling patterns, especially those driven by exogenous forces, can result in biases to standardized abundance indices. Within the range of scenarios that were considered in the present study, the *Rotating*, *Preferential* and *Contraction* (if sampling covered at least ~ 20 − 40% of the target spatial domain) spatial sampling scenarios performed comparably to the baseline *Random* sampling pattern indicating that spatiotemporal delta-GLMMs may still be appropriate to use if the departure from uniform, random sampling is not too extreme. However, the simulations conducted in the present study also demonstrated that even when the estimation model matched the induced catchability effects on positive catch-rates, estimation models developed under the *Random* sampling scenario were not able to completely remove the effects of temporal changes in catchability and produce an unbiased abundance index. Although the resulting abundance indices were not perfect, models were generally able to disentangle temporal changes in abundance due to spatial shifts from temporal changes in catchability, provided that the spatial shifts were not too severe. Lastly, in the context of the simulation experiment, inclusion of environmental covariates or climatic indices via SVC in the spatiotemporal model did not appear to improve model performance beyond the standard model configuration including only spatial and spatiotemporal random effects. However, this could be due to the tropical focus of the simulation and case-study as a more pronounced impact is seen in temperate fisheries with perhaps greater seasonal variability (Thorson, 2019b).

The simulations explored in the current study indicate that the bias and error associated with preferential sampling are not manifested in a binary sense, but rather exist on a continuum. The expected result is that when data generated from preferential sampling is used to create an abundance index, it will not be representative of the underlying

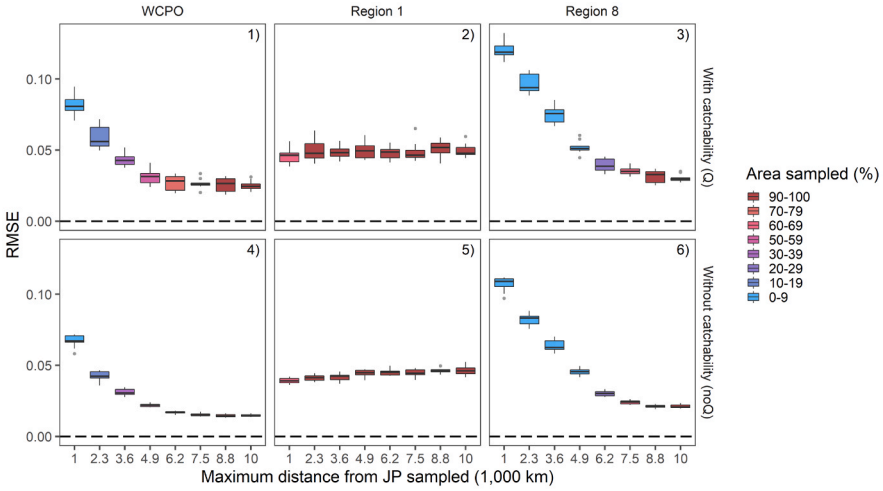

(a) RMSE

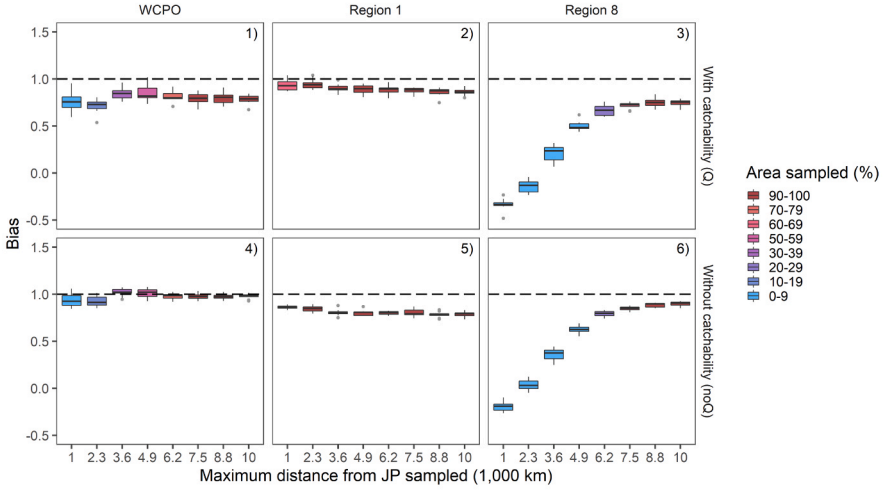

(b) Bias

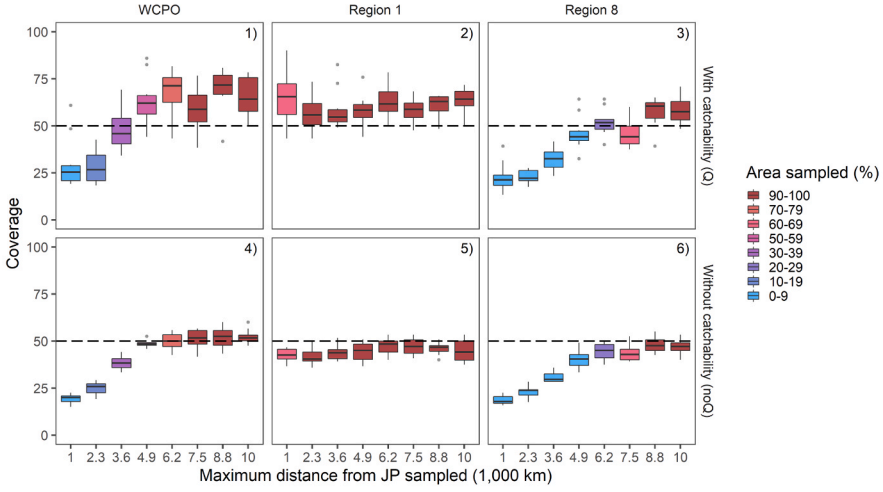

(c) Coverage

Fig. 6. Summary of the three metrics considered in this study, a) root mean squared error (RMSE), b) bias, and c) confidence interval coverage for the sensitivity to the degree of spatial contraction (see Section 2.1.5 for a description of the metrics). Within each group of figures, the rows correspond to the models fit with and without catchability, while the columns correspond to results from select model regions: the western and central Pacific Ocean (WCPO), Region 1 (closest to Japan (JP) and temporally well sampled), and Region 8 (furthest from Japan and most sensitive to sampling effort contraction). Within each panel the box-plots are arranged in terms of decreasing simulated spatial contraction (left to right), and are colored according to the proportion of the area sampled in the final time-steps of the simulation. Note that the degree of spatial contraction does not change linearly across the x-axis.

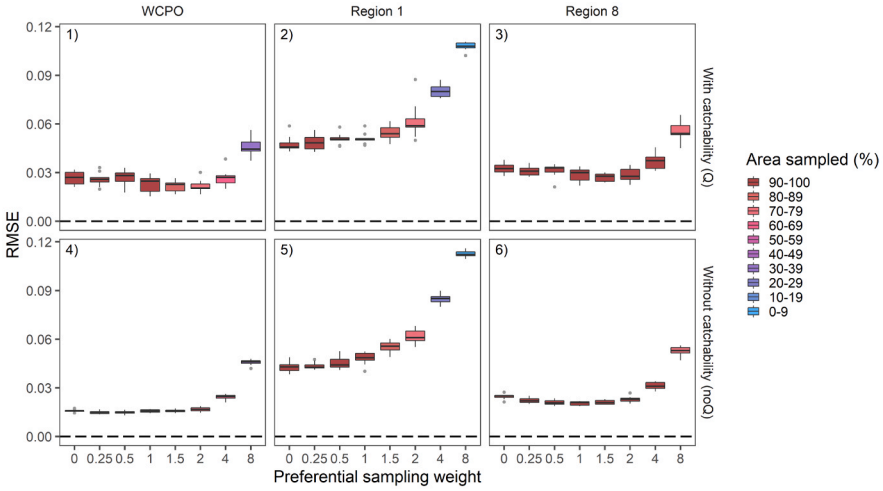

(a) RMSE

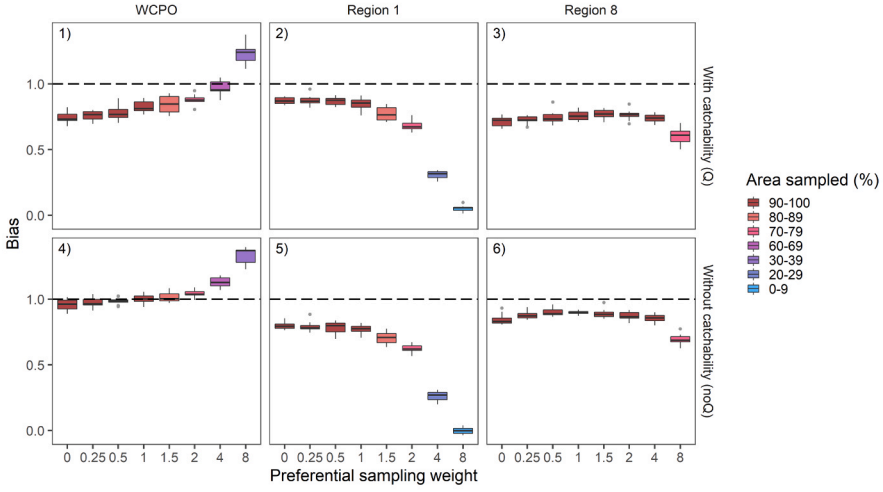

(b) Bias

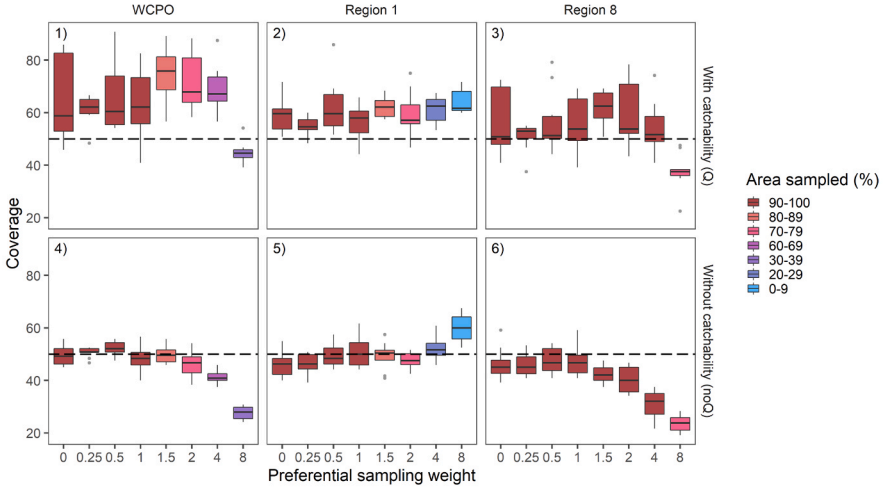

(c) Coverage

Fig. 7. Summary of the three metrics a) RMSE, b) Bias, and c) Coverage for the sensitivity to the degree of preferential sampling. Within each group of figures, the rows correspond to the models fit with and without catchability, while the columns correspond to results from select model regions: WCPO, Region 1 (closest to Japan and on the fringe of the SEAPODYM skipjack distribution), and Region 8 (furthest from Japan and closer to the core of the SEAPODYM skipjack distribution). Within each panel the box-plots are arranged in terms of increasing simulated preferential sampling strength (left to right), and are colored according to the proportion of the area sampled. Note that a non-linear transformation has been applied to the x-axis.

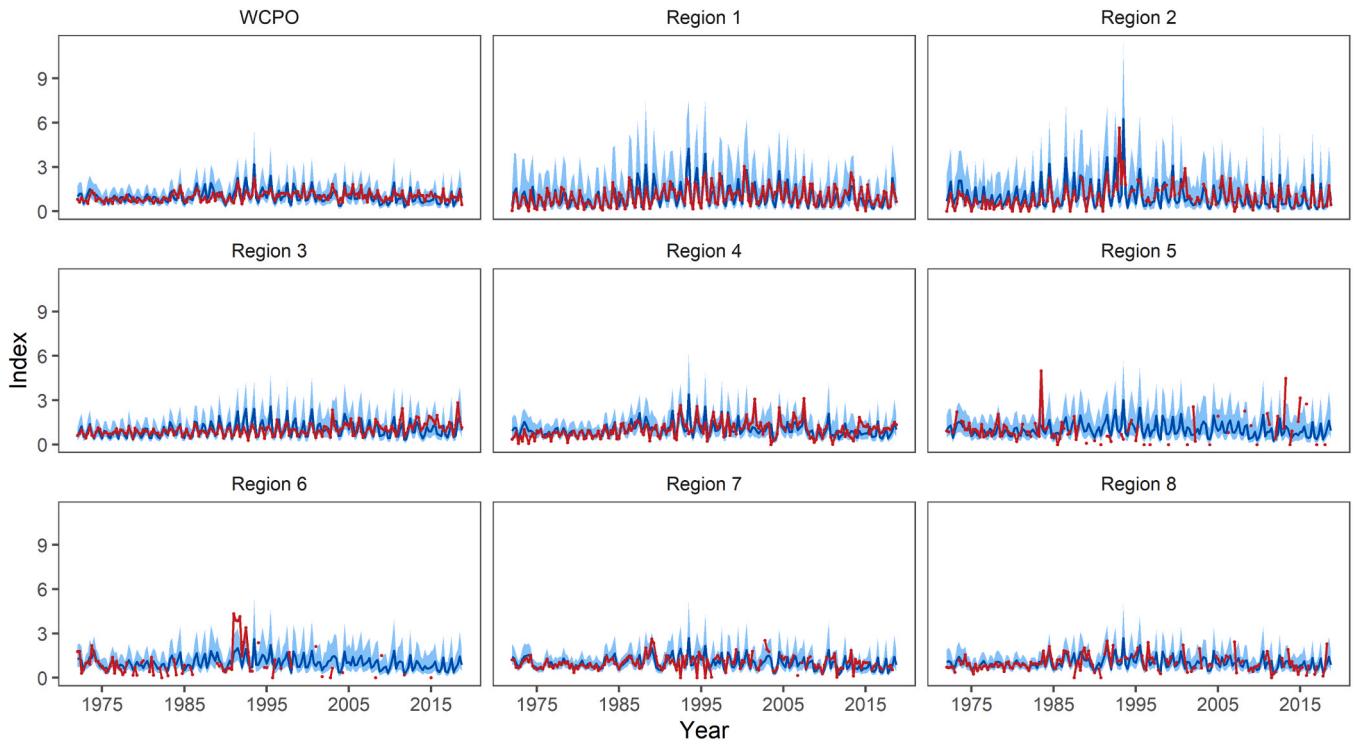

Fig. 8. Estimated skipjack tuna (*Katsuwonus pelamis*) relative abundance indices for each of the western and central Pacific Ocean (WCPO) stock assessment regions from the Japanese pole-and-line fishery from the *ESVC* model. Relative nominal catch-per-unit-effort (CPUE) is shown by the black dots. The blue line indicates the standardized abundance index, with the shaded region showing the 95% confidence interval. All variables displayed were standardized to a mean of 1 for plotting. The *ESVC* model consisted of the baseline spatio-temporal model described in Section 2.2.2 with a linear effect of sea-surface temperature on skipjack tuna abundance and an index of the Niño 4 temperature anomalies included as a spatially-varying coefficient (SVC).

population (Diggle et al., 2010; Conn et al., 2017). Though this is undoubtedly true in situations of extreme preferential sampling such as the one explored in (Pennino et al., 2019), it is not always the case. Models fit to data with weak preferential sampling (e.g *Preferential* scenario) performed as well or better than models fit to data from *Random* sampling. The sensitivity experiment manipulating the preferential sampling intensity appeared to illustrate a slight trade-off between sampling at the core of the abundance distribution versus completely sampling the entire range of the underlying species when preferential sampling was weak. However, a caveat to this finding is that this trade-off is likely only applicable in cases where the underlying abundance distribution is temporally stable. Non-stationarity or range contraction in the species' abundance distribution coupled with preferential sampling would likely lead to increased bias and error, relative to random sampling, even in cases where preferential sampling is weak. As a result the spatiotemporal distribution of samples should be carefully scrutinized in the context of the perceived underlying abundance distribution prior to estimating abundance indices using spatiotemporal models.

Fisheries-dependent data are typically spatially imbalanced, as fishers usually target rather than randomly sample fish populations (Walters, 2003; Maunder and Punt, 2004; Lynch et al., 2012). In this context, caution is warranted regarding the specifications of spatiotemporal models fitted to fisheries-dependent data. One primary means of dealing with spatially-imbalanced fisheries-dependent data is to proceed as we did in the present study and allocate the "knots" for approximating spatial and spatiotemporal variation terms uniformly over space using a predefined spatial grid, rather than based on fishing intensity using a *k*-means algorithm (Grüss et al., 2019). Additional means of dealing with spatially-imbalanced, fisheries-dependent data are the use of a "bias-correction estimator" (Thorson and Kristensen, 2016), and employing a first-order autoregressive structure across time for the spatiotemporal variation terms (Thorson, 2019a). The very large number of data points and scenarios handled in the present study precluded us from implementing these two additional options within reasonable computation time, but we recommend that future studies working with smaller datasets consider them. The bias-correction estimator developed in Thorson and Kristensen (2016)) is useful to correct for the "retransformation bias" when one predicts a derived quantity that involves a non-linear transformation of the random effects. A first-order autoregressive structure across time for the spatiotemporal variation terms allows for the estimation of abundance in unfished areas based on predicted abundance for these areas in adjacent years rather than based on a long-term predicted average abundance for these areas (Thorson, 2019a). Future work with fisheries-dependent data where preferential sampling is taking place should consider exploring a joint model for fishing location and density such as the marked point process model applied by (Pennino et al., 2019). This would be feasible in a framework such as *VAST* by specifying both variables in a multivariate model where, for example, an estimated positive correlation would extrapolate lower densities in areas with few or no sampling data (all else being equal).

An explicit caveat should be made that unlike other fisheries-dependent CPUE standardization work (Carruthers et al., 2010, 2011) this work does not describe a fully closed simulation, where fishing or *sampling* in this case influences the underlying population dynamics. As a result, an implicit assumption is made that *sampling* or removals from the system are too small to impact the overall abundance distribution and that localized depletion does not occur. While this assumption may be plausible to make in the case of a highly migratory species occupying a dynamic pelagic environment such as skipjack tuna, further research should be conducted to examine the implications of extending these findings in a closed simulation to fisheries and species, such as demersal groundfish or reef fish, where localized depletion could be a concern.

Given the structure of the WCPFC skipjack tuna stock assessment (Vincent et al., 2019), the analyses carried out in the present study explored estimating abundance indices at a quarterly time step rather

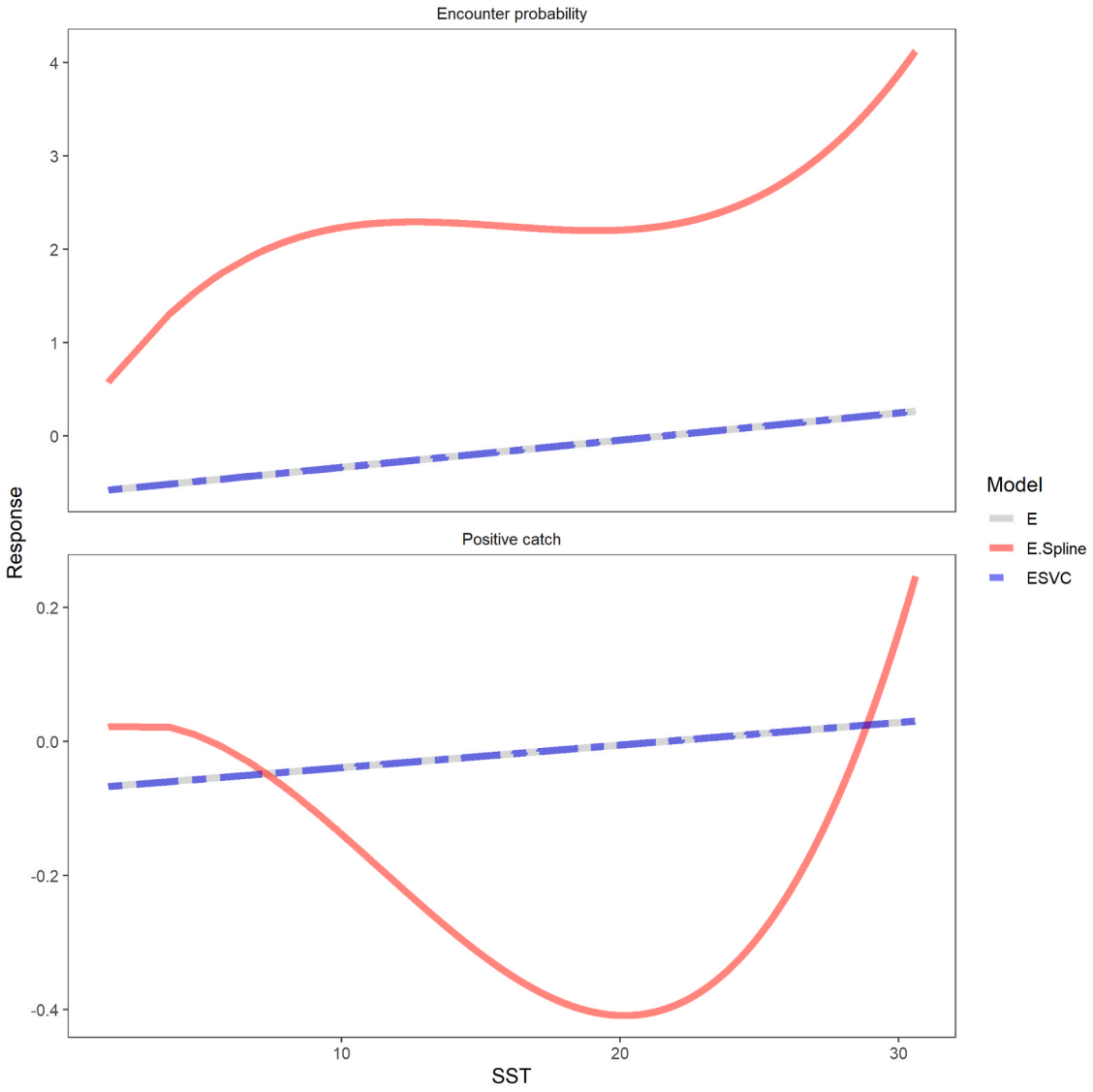

Fig. 9. Estimated environmental relationship between sea surface temperature (SST) and skipjack tuna (*Katsuwonus pelamis*) by model component, encounter probability and positive catch-rate, for three different standardization models: *E*, *E.Spline*, and *ESVC*. All three models were based off the baseline spatio-temporal model described in Section 2.2.2. The *E* model included a linear effect of sea-surface temperature (SST) on skipjack tuna abundance, the *E.Spline* model included a non-linear effect of SST on abundance as a cubic spline, and the *ESVC* model added the linear effect of SST and an index of the Niño 4 temperature anomalies included as a spatially-varying coefficient (SVC).

than estimating an annual index with the quarterly effect removed via its inclusion as a catchability factor in the spatiotemporal model (Grüss et al., 2019). In the context of the fishery application considered in the present study, additional work is warranted to explore how structured seasonal, spatiotemporal models (Thorson et al., 2020a) could result in an improved abundance index, especially if the high intra-annual variation observed in the current study is a product of seasonal specific fishing patterns. More generally given the poor performance of models in the *Fixed* scenario considered in this study, which noticeably struggled when a portion of the underlying stock went consistently un-sampled, application of a model with structured intra-annual correlation could produce an abundance index with reduced error and improved confidence interval coverage.

As mentioned in Section 3.2, the JPPL abundance index appears to be relatively constant over the modeled period and, in model regions that are well sampled, it does not deviate greatly from the nominal CPUE. It is possible that the standardized abundance index does not vary in proportion to the population trend of the target skipjack tuna stock. Logbook catch data for the JPPL fishery is recorded as metric tons caught per day, without mention of the number of schools encountered and/or the size of the schools fished. This format of data reporting could be intrinsically hyperstable by inadvertently obscuring potential effects of gear/vessel saturation (ArreguinSanchez, 1996; Kuriyama et al., 2019) and searching behavior for schools (Gaertner and Dreyfus-Leon, 2004). For instance, 10 mt harvested from the edge of a 100 mt school could imply something different in terms of the population health than 10 mt harvested by completely capturing 5 separate 2 mt schools. Information on the search time, school size, number of schools fished per day, or school association (i.e. associated with natural floating object or fish-aggregating device) could reduce the risk of hyperstability in the abundance index.

The spatial distribution of skipjack tuna is known to be influenced by the location of the convergence zone on the eastern extent of the WCPO Warm Pool (Lehodey et al., 1997). When the Warm Pool expands during "El Niño" phases skipjack tuna typically range further east while they tend to remain more concentrated in the equatorial western Pacific during "La Niña" phases. Investigation of the spatial distribution of the estimated SVC random effects for both encounter-rate and positive

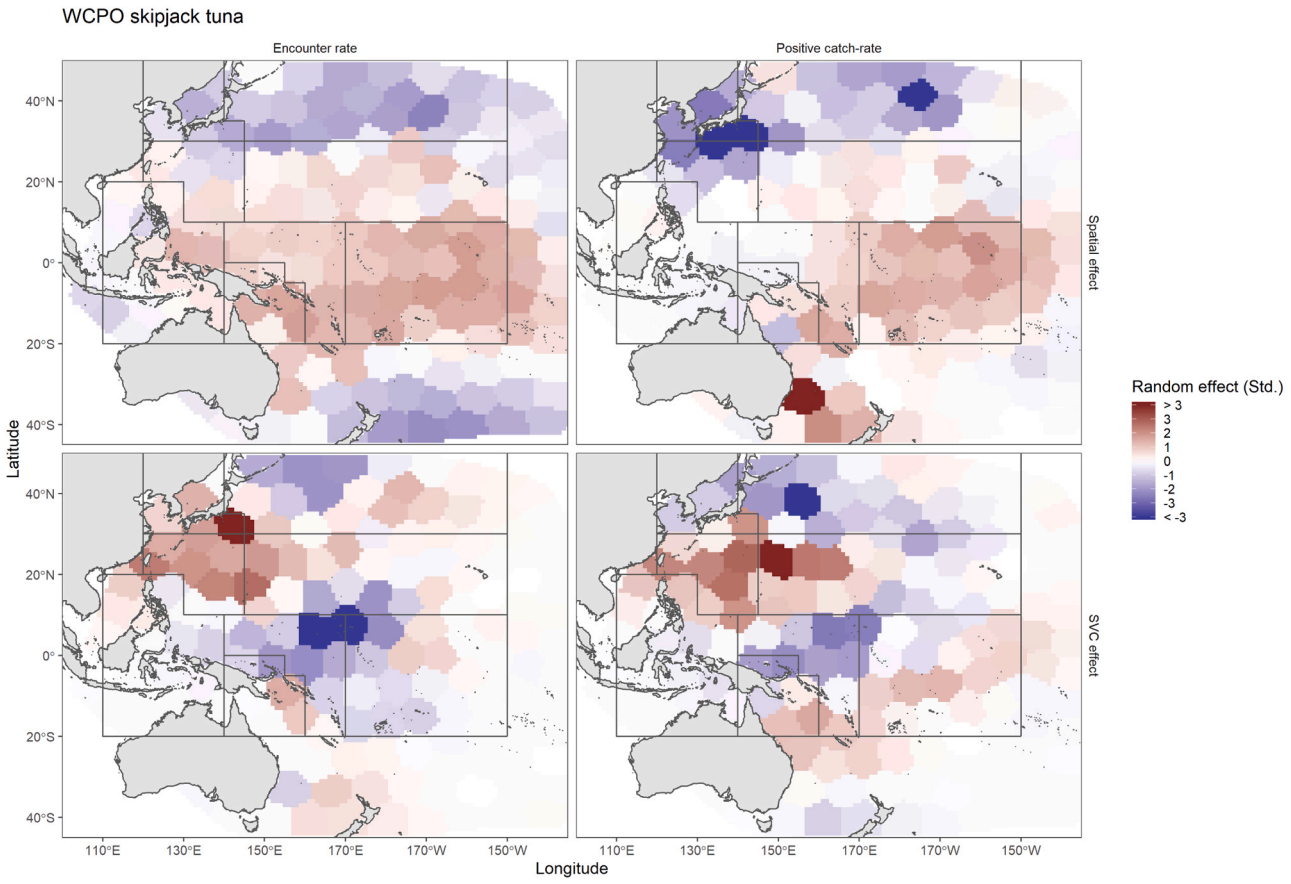

Fig. 10. Estimated spatial and spatially-varying coefficient (SVC) random effects by model component, encounter probability and positive catch-rate, from the *ESVC* model. The *ESVC* model consisted of the baseline spatio-temporal model described in Section 2.2.2 with a linear effect of sea-surface temperature on skipjack tuna abundance and an index of the Niño 4 temperature anomalies included as an SVC.

catch-rate appear to support this temporal pattern. Within the equatorial WCPO, positive random effects (indicating a positive correlation with "El Niño" phases) are located to the east while negative random effects (indicating a positive correlation with La Niña phases) are located towards the west (Fig. 10 bottom-right). Outside of the equatorial WCPO and the Warm Pool, there appears to be a strong positive correlation with "El Niño" phases in the north-west Pacific Ocean between typical locations of the Kuroshio Extension current and the North Equatorial current. Though the effect of Southern Oscillation Index phases on skipjack distribution and abundance are less well studied outside of the equatorial Pacific Ocean, this observation makes sense in the context of existing oceanographic research that found that the North Equatorial current undergoes a northward shift during "El Niño" phases (Qiu, 2001). A northern shift of this warm-water current and associated fronts could aggregate skipjack forage such as plankton and micronekton in an otherwise less productive area and could explain the higher catches and encounter-rates seen during "El Niño" phases.

In the JPPL fisheries application considered in this study (Section 2.2.2), high catches were recorded at "low" temperatures particularly near the Kuroshio Extension current. There are two potential explanations for this observation. The Kuroshio Extension is a highly dynamic and productive system (Kimura, 2000), characterized by a meandering jet (Mizuno and White, 1983) and warm-core eddies (Yasuda et al., 1992), where warm, tropical waters shoal above cold, temperate waters from the Oyashio Current. If vessels are targeting these mesoscale features, it is likely that they are not actually fishing in waters below 18°C and that the "observed" cold temperatures result from a mismatch between the spatial and temporal resolutions of the fishing sets (daily, 1°) and the SST observations (quarterly, 2°). Indeed, high resolution (daily, 1/12°) data covering the Kuroshio Extension area from the Japan Coastal Ocean Predictability Experiment 2 (JCOPE2; Miyazawa et al., 2009) showed that quarterly 2° cells with average temperatures as low as 7. 8°C could still contain viable skipjack tuna habitat. This suggests that future research could explore fitting alternative features that arise from aggregating high-resolution covariate data (e.g. SST) to the spatial scale of the estimation model. Future examples to explore include maximum or upper quantile of SST, the area covered by mesoscale eddies, metrics of horizontal SST differential or other such features that more accurately capture tuna habitat selection than broad-scale average temperature. Additionally, Kiyofuji et al. (2019)) showed that the vertical distribution of tagged skipjack became shallower within the Kuroshio Extension area as a result of thermal compression due to the subsurface cold water mass from the Oyashio current. The thermal compression of skipjack in the Kuroshio Extension area could make skipjack schools easier to locate, and more accessible to the surface-oriented pole-and-line gear resulting in larger catches at these "observed" cold temperatures. Future studies on this system should try and explicitly account for the effects of thermal compression on skipjack tuna catchability. Finally, the biological operating model (SEAPODYM) includes a bottom-up effect of environmental conditions on fish biomass, such that SST (and by extension ENSO) affect density in the estimation model. However, as just mentioned, environmental conditions could alternatively affect catchability (e.g., where warm water causes a greater overlap in vertical distribution with accessibility to pole-and-line fishing), and it typically requires process research (focused experiments or complementary sampling methods) to identify whether covariates affect catchability or density. We did not explore a simulation scenario involving mis-specification (e.g., where a covariate affects catchability in the operating model but density in the

estimation model), and note this as a topic for future research.

Though the analyses conducted in the present study shows that, in certain scenarios, spatiotemporal delta-GLMMs could still be appropriate to use for the standardization of fisheries-dependent data, there is still opportunity for future research in this area. Recent developments to the *VAST* modeling framework (release number > 3.6.0) have made it possible to specify separate catchability and environmental covariates for the two different model components of the delta-GLMM: encounter probability and positive catch-rate. Taking advantage of this functionality and specifying separate covariate structures could remove inadvertent model mis-specification caused by differential covariate effects between the two model components. Additionally, this paper considered a single-species approach to modeling fisheries-dependent data, yet spatiotemporal delta-GLMMs can easily be extended to a multi-species framework (Thorson, 2017). By explicitly accounting for the covariance between species, there is the potential to improve abundance indices in mixed-fisheries by using the abundance of one species to gain additional information on the other (Thorson et al., 2016). This should be explored in the context of the JPPL fishery as it also opportunistically targets schools of north Pacific albacore tuna (*Thunnus alalunga*) in the Kuroshio Extension area (Kimura and Sugimoto, 1997; Kiyofuji, 2013). A high-resolution analysis of the catch-rate data partitioned between skipjack tuna and albacore tuna could identify trade-offs in the abundance dynamics of the two target species as it relates to phases in Kuroshio Extension variability.

CRediT authorship contribution statement

Nicholas D. Ducharme-Barth: Conceptualization, Methodology, Software, Formal Analysis, Visualization, Writing - Review & Editing. **Arnaud Grüss:** Conceptualization, Methodology, Writing - Original Draft, Writing - Review & Editing. **Matthew T. Vincent:** Conceptualization, Writing - Review & Editing. **Hidetada Kiyofuji:** Conceptualization, Writing - Review & Editing. **Yoshinori Aoki:** Conceptualization, Writing - Review & Editing. **Graham Pilling:** Conceptualization, Writing - Review & Editing. **John Hampton:** Conceptualization, Writing - Review & Editing. **James T. Thorson:** Conceptualization, Writing - Original Draft, Writing - Review & Editing.

Declaration of Competing Interest

The authors declare that they have no known competing financial interests or personal relationships that could have appeared to influence the work reported in this paper.

Acknowledgments

The scientific results and conclusions, as well as any views or opinions expressed herein, are those of the authors and do not necessarily reflect those of National Oceanic and Atmospheric Administration (NOAA), the Department of Commerce, Pacific Community (SPC), the National Institute of Water and Atmospheric Research, the University of Washington, and the Japan Fisheries Research and Education Agency. The authors would like to thank those whose insightful discussion contributed to the manuscript: J. Macdonald (SPC), T. Vidal (SPC), and J. Kinoshita (National Research Institute Far Seas Fisheries; NRIFSF). Additionally, we gratefully appreciate the time given by the following reviewers for improving the quality of this manuscript with their comments: P. Hamer (SPC), M. Karp (NOAA), H. Xu (Inter-American Tropical Tuna Commission; IATTC), B. Alglave (Agrocampus Ouest), and two anonymous reviewers.

This research did not receive any specific grant from funding agencies in the public, commercial, or not-for-profit sectors.

Appendix A. Supporting information

Supplementary data associated with this article can be found in the online version at doi:10.1016/j.fishres.2021.106169.

References

Agresti, A., Coull, B.A., 1998. Approximate is better than "Exact" for interval estimation of binomial proportions. In: The American Statistician, 52, p. 119. https://doi.org/10.2307/2685469.

Allen, P.M., McGlade, J.M., . 1986. Dynamics of discovery and exploitation: the case of the Scotian shelf groundfish fisheries. Can. J. Fish. Aquat. Sci. 43 (6), 1187–1200. ⟨http://www.nrcresearchpress.com/doi/10.1139/f86-148⟩.

ArreguinSanchez, F., 1996. Catchability: A key parameter for fish stock assessment. Rev. Fish. Biol. Fish. 6 (2), 221–242. ://WOS:A1996UV07400005.

Bishop, J., Venables, W.N., Wang, Y.G., 2004. Analysing commercial catch and effort data from a penaeid trawl fishery - A comparison of linear models, mixed models, and generalised estimating equations approaches. Fish. Res. 70 (2–3), 179–193. https://doi.org/10.1016/j.fishres.2004.08.003.

Bolker, B., 2008. Ecological models and data in R. Princeton University Press, Princeton, NJ.

Branch, T.A., Hilborn, R., 2008. Matching catches to quotas in a multispecies trawl fishery: targeting and avoidance behavior under individual transferable quotas. Can. J. Fish. Aquat. Sci. 65 (7), 1435–1446. https://doi.org/10.1139/F08-065.

Brown, L.D., Cai, T.T., DasGupta, A., 2001. Interval estimation for a binomial proportion. Stat. Sci. 16 (2), 101–133. https://doi.org/10.1214/ss/1009213286. ⟨http://projecteuclid.org/euclid.ss/1009213286⟩.

Campbell, R.A., 2004. CPUE standardisation and the construction of indices of stock abundance in a spatially varying fishery using general linear models. Fish. Res. 70 (2–3), 209–227. https://doi.org/10.1016/j.fishres.2004.08.026.

Campbell, R.A., 2015. Constructing stock abundance indices from catch and effort data: Some nuts and bolts. Fish. Res. 161, 109–130. https://doi.org/10.1016/j.fishres.2014.07.004.

Cao, J., Thorson, J.T., Richards, R.A., Chen, Y., 2017. Spatiotemporal index standardization improves the stock assessment of northern shrimp in the Gulf of Maine. Can. J. Fish. Aquat. Sci. 74, 1781–1793. https://doi.org/10.1139/cjfas-2016-0137.

Carruthers, T.R., Ahrens, R.N.M., McAllister, M.K., Walters, C.J., 2011. Integrating imputation and standardization of catch rate data in the calculation of relative abundance indices. Fish. Res. 109, 157–167. https://doi.org/10.1016/j.fishres.2011.01.033.

Carruthers, T.R., McAllister, M.K., Ahrens, R.N.M., 2010. Simulating spatial dynamics to evaluate methods of deriving abundance indices for tropical tunas. Can. J. Fish. Aquat. Sci. 67, 1409–1427. https://doi.org/10.1139/f10-056.

Clark, C.W., Mangel, M., 1979. Aggregation and fishery dynamics - theoretical study of schooling and the purse seine tuna fisheries. Fish. Bull. 77, 317–337.

Cochran, W.G., 1977. Sampling techniques. Wiley Series In Probability and Mathematical Statistics, 3rd ed..,. Wiley,, New York.

Conn, P.B., Thorson, J.T., Johnson, D.S., 2017. Confronting preferential sampling when analysing population distributions: diagnosis and model-based triage. Methods Ecol. Evol. 8, 1535–1546. https://doi.org/10.1111/2041-210X.12803. ⟨https://onlinelibrary.wiley.com/doi/abs/10.1111/2041-210X.12803⟩.

Dennis, D., Plagányi, v., Van Putten, I., Hutton, T., Pascoe, S., 2015. Cost benefit of fishery-independent surveys: Are they worth the money? Mar. Policy 58, 108–115. https://doi.org/10.1016/j.marpol.2015.04.016. ⟨https://linkinghub.elsevier.com/retrieve/pii/S0308597×15000986⟩.

Deriso, R.B., Parma, A.M., 1987. On the odds of catching fish with angling gear. Trans. Am. Fish. Soc. 116, 244–256. https://doi.org/10.1577/1548-8659(1987)116<244:otoocf>2.0.co;2.

Diggle, P., Menezes, R., Su, T.-I., 2010. Geostatistical inference under preferential sampling. J. R. Stat. Soc.: Ser. C. (Appl. Stat.) 59, 191–232. https://doi.org/10.1111/j.1467-9876.2009.00701.x.

Ducharme-Barth, N., & Vincent, M., 2020). Analysis of Pacific-wide operational longline dataset for bigeye and yellowfin tuna catch-per-unit-effort (CPUE). Technical Report WCPFC-SC16–2020/SC16-SA-IP-07.

Ducharme-Barth, N.D., Shertzer, K.W., Ahrens, R.N., 2018. Indices of abundance in the Gulf of Mexico reef fish complex: A comparative approach using spatial data from vessel monitoring systems. Fish. Res. 198, 13.

Eigaard, O.R., Marchal, P., Gislason, H., Rijnsdorp, A.D., 2014. Technological development and fisheries management. Rev. Fish. Sci. Aquac. 22, 156–174. https://doi.org/10.1080/23308249.2014.899557. ⟨http://www.tandfonline.com/doi/abs/10.1080/23308249.2014.899557⟩.

Gaertner, D., Dreyfus-Leon, M., 2004. Analysis of non-linear relationships between catch per unit effort and abundance in a tuna purse-seine fishery simulated with artificial neural networks. ICES J. Mar. Sci. 61, 812–820. https://doi.org/10.1016/j.icesjms.2004.05.002. ⟨https://academic.oup.com/icesjms/article/61/5/812/867451⟩.

Girardin, R., Hamon, K.G., Pinnegar, J., Poos, J.J., Thébaud, O., Tidd, A., Vermard, Y., Marchal, P., 2017. Thirty years of fleet dynamics modelling using discrete-choice models: What have we learned? Fish Fish 18, 638–655. https://doi.org/10.1111/faf.12194. ⟨http://doi.wiley.com/10.1111/faf.12194⟩.

Grüss, A., Walter, J.F., Babcock, E.A., Forrestal, F.C., Thorson, J.T., Lauretta, M.V., Schirripa, M.J., 2019. Evaluation of the impacts of different treatments of spatio-temporal variation in catch-per-unit-effort standardization models. Fish. Res. 213,

75–93. https://doi.org/10.1016/j.fishres.2019.01.008. ⟨https://linkinghub.elsevier.com/retrieve/pii/S0165783619300086⟩.
Han, Q., Grüss, A., Shan, X., Jin, X., Thorson, J.T., 2021. Understanding patterns of distribution shifts and range expansion/contraction for small yellow croaker (Larimichthys polyactis) in the yellow sea. Fish. Oceanogr. 30, 69–84. https://doi.org/10.1111/fog.12503 (arXiv). ⟨https://onlinelibrary.wiley.com/doi/pdf/10.1111/fog.12503⟩.
Harley, S.J., Myers, R.A., Dunn, A., 2001. Is catch-per-unit-effort proportional to abundance? ://WOS:000170811300007 Can. J. Fish. Aquat. Sci. 58, 1760–1772. https://doi.org/10.1139/cjfas-58-9-1760.
Hijmans, R.J. (2019). geosphere: Spherical trigonometry. version 1.5–10.⟨https://CRAN.R-project.org/package=geosphere⟩.
Hilborn, R., Walters, C.J., 1987. A general model for simulation of stock and fleet dynamics in spatially heterogeneous fisheries. Can. J. Fish. Aquat. Sci. 44, 1366–1369. https://doi.org/10.1139/f87-163. ⟨http://www.nrcresearchpress.com/doi/10.1139/f87-163⟩.
Holland, D.S., 2000. A bioeconomic model of marine sanctuaries on Georges Bank. Can. J. Fish. Aquat. Sci. 57, 1307–1319. https://doi.org/10.1139/f00-061. ⟨http://www.nrcresearchpress.com/doi/10.1139/f00-061⟩.
Johnson, K.F., Councill, E., Thorson, J.T., Brooks, E., Methot, R.D., Punt, A.E., 2016. Can autocorrelated recruitment be estimated using integrated assessment models and how does it affect population forecasts? Fish. Res. 183, 222–232. https://doi.org/10.1016/j.fishres.2016.06.004. ⟨https://linkinghub.elsevier.com/retrieve/pii/S0165783616301928⟩.
Kass, R.E., Steffey, D., 1989. Approximate bayesian inference in conditionally independent hierarchical models (parametric empirical bayes models). J. Am. Stat. Assoc. 84, 717–726. https://doi.org/10.1080/01621459.1989.10478825. ⟨https://www.tandfonline.com/doi/full/10.1080/01621459.1989.10478825⟩.
Kimura, S., 2000. Biological production in meso-scale eddies caused by frontal disturbances of the Kuroshio Extension. ICES J. Mar. Sci. 57, 133–142. https://doi.org/10.1006/jmsc.1999.0564. ⟨https://academic.oup.com/icesjms/article-lookup/doi/10.1006/jmsc.1999.0564⟩.
Kimura, S., Sugimoto, M.N.A.T., 1997. Migration of albacore, Thunnus alalunga, in the North Pacific Ocean in relation to large oceanic phenomena. Fish. Oceanogr. 6, 51–57. https://doi.org/10.1046/j.1365-2419.1997.00029.x. ⟨http://doi.wiley.com/10.1046/j.1365-2419.1997.00029.x⟩.
Kinoshita, J., Aoki, Y., Ducharme-Barth, N., Kiyofuji, H.2019. Standardized catch per unit effort (CPUE) of skipjack tuna of the Japanese pole-and-line fisheries in the WCPO from 1972 to 2018. Technical Report WCPFC-SC15–2019/SA-WP-14 Pohnpei, Federated States of Micronesia.
Kiyofuji, H. (2013). Reconsideration of CPUE for albacore caught by the Japanese pole and line fishery in the northwestern North Pacific Ocean. Technical Report ISC/13/ALBWG-01/11.
Kiyofuji, H. (2016). Skipjack catch per unit effort (CPUE) in the WCPO from the Japanese pole-and-line fisheries. Technical Report WCPFC-SC12–2016/SA-WP-05 Bali, Indonesia, 3–11 August 2016.
Kiyofuji, H., Aoki, Y., Kinoshita, J., Okamoto, S., Masujima, M., Matsumoto, T., Fujioka, K., Ogata, R., Nakao, T., Sugimoto, N., Kitagawa, T., 2019. Northward migration dynamics of skipjack tuna (Katsuwonus pelamis) associated with the lower thermal limit in the western Pacific Ocean. Prog. Oceanogr. 175, 55–67. https://doi.org/10.1016/j.pocean.2019.03.006. ⟨http://www.sciencedirect.com/science/article/pii/S007966111830185X⟩.
Kiyofuji, H., Uosaki, K., & Hoyle, S. (2011). Up-to-date CPUE for skipjack caught by Japanese distant and offshore pole and line in the western central Pacific Ocean. Technical Report WCPFC-SC7–2011/SA-IP-13 Pohnpei, Federated States of Micronesia.
Kotwicki, S., Ono, K., 2019. The effect of random and density-dependent variation in sampling efficiency on variance of abundance estimates from fishery surveys (p. faf.12375). Fish Fish. https://doi.org/10.1111/faf.12375 (p. faf.12375). ⟨https://onlinelibrary.wiley.com/doi/abs/10.1111/faf.12375⟩.
Kuriyama, P.T., Branch, T.A., Hicks, A.C., Harms, J.H., Hamel, O.S., 2019. Investigating three sources of bias in hook-and-line surveys: survey design, gear saturation, and multispecies interactions. Can. J. Fish. Aquat. Sci. 76, 192–207. https://doi.org/10.1139/cjfas-2017-0286. ⟨http://www.nrcresearchpress.com/doi/10.1139/cjfas-2017-0286⟩.
Langley, A., Uosaki, K., Hoyle, S., Shono, H., & Ogura, M. (2010). A standardized CPUE analysis of the Japanese distant-water skipjack pole-and-line fishery in the western and central Pacific Ocean (WCPO), 1972–2009. Technical Report WCPFC-SC6–2010/SA-WP-08.
Lehodey, P., Bertignac, M., Hampton, J., Lewis, A., Picaut, J., 1997. El Niño Southern Oscillation and tuna in the western Pacific. Nature 389, 715–718. https://doi.org/10.1038/39575. ⟨http://www.nature.com/articles/39575⟩.
Lehodey, P., Bertrand, A., Hobday, A.J., Kiyofuji, H., McClatchie, S., Menkés, C.E., Pilling, G., Polovina, J., Tommasi, D., 2020. Enso impact on marine fisheries and ecosystems (American Geophysical Union (AGU)). El Niño South. Oscil. a Chang. Clim. Chapter 19 429–451. https://doi.org/10.1002/9781119548164.ch19 (arXiv). ⟨https://AGUpubs.onlinelibrary.wiley.com/doi/pdf/10.1002/9781119548164.ch19⟩.
Lehodey, P., Senina, I., Murtugudde, R., 2008. A spatial ecosystem and populations dynamics model (SEAPODYM) - Modeling of tuna and tuna-like populations. Prog. Oceanogr. 78, 304–318. https://doi.org/10.1016/j.pocean.2008.06.004. ⟨https://linkinghub.elsevier.com/retrieve/pii/S007966110800116X⟩.
Lo, N.C.H., Jacobson, L.D., Squire, J.L., 1992. Indexes of relative abundance from fish spotter data based on delta-lognormal models. ://WOS:A1992KL53200010 Can. J. Fish. Aquat. Sci. 49, 2515–2526. https://doi.org/10.1139/f92-278.
Lynch, P.D., Shertzer, K.W., Latour, R.J., 2012. Performance of methods used to estimate indices of abundance for highly migratory species. ://WOS:000304849100004 Fish. Res. 125, 27–39. https://doi.org/10.1016/j.fishres.2012.02.005.
Maunder, M.N., Punt, A.E., 2004. Standardizing catch and effort data: a review of recent approaches. ://WOS:000225943700002 Fish. Res. 70, 141–159. https://doi.org/10.1016/j.fishres.2004.08.002.
Maunder, M.N., Thorson, J.T., Xu, H., Oliveros-Ramos, R., Hoyle, S.D., Tremblay-Boyer, L., Lee, H.H., Kai, M., Chang, S.-K., Kitakado, T., Albertsen, C.M., Minte-Vera, C.V., Lennert-Cody, C.E., Aires-da Silva, A.M., Piner, K.R., 2020. The need for spatio-temporal modeling to determine catch-per-unit effort based indices of abundance and associated composition data for inclusion in stock assessment models. Fish. Res. 229, 105594 https://doi.org/10.1016/j.fishres.2020.105594. ⟨https://linkinghub.elsevier.com/retrieve/pii/S0165783620301119⟩.
Miyazawa, Y., Zhang, R., Guo, X., Tamura, H., Ambe, D., Lee, J.-S., Okuno, A., Yoshinari, H., Setou, T., Komatsu, K., 2009. Water mass variability in the western North Pacific detected in a 15-year eddy resolving ocean reanalysis. J. Oceanogr. 65, 737–756. https://doi.org/10.1007/s10872-009-0063-3. ⟨http://link.springer.com/10.1007/s10872-009-0063-3⟩.
Mizuno, K., White, W., 1983. Annual and Interannual Variability in the Kuroshio Current System. J. Phys. Oceanogr. 13, 1847–1867.
Moore, B.R., Bell, J.D., Evans, K., Farley, J., Grewe, P.M., Hampton, J., Marie, A.D., Minte-Vera, C., Nicol, S., Pilling, G.M., ScuttPhillips, J., Tremblay-Boyer, L., Williams, A.J., Smith, N., 2020. Defining the stock structures of key commercial tunas in the Pacific Ocean I: Current knowledge and main uncertainties. Fish. Res. 230, 105525 https://doi.org/10.1016/j.fishres.2020.105525. ⟨https://linkinghub.elsevier.com/retrieve/pii/S0165783620300424⟩.
Newcombe, R., 1998. Two-sided confidence intervals for the single proportion: comparison of seven methods. Stat. Med. 17, 857–872, 10.1002/(SICI)1097-0258(19980430)17:8<857::AID-SIM777>3.0.CO;2-E.
Ogura, M., & Shono, H. (1999a). Factors affecting the fishing effort of the Japanese distant water pole and line vessel and the standardization of that skipjack CPUE - Part A Description of the fishery and data. Technical Report SCTB12.
Ogura, M., & Shono, H. (1999b). Factors affecting the fishing effort of the Japanese distant water pole and line vessel and the standardization of that skipjack CPUE. Part B - Calculation of CPUE standardization. Technical Report SCTB12.
Pennino, M.G., Paradinas, I., Illian, J.B., Muñoz, F., Bellido, J.M., López-Quílez, A., Conesa, D., 2019. Accounting for preferential sampling in species distribution models. Ecol. Evol. 9, 653–663. https://doi.org/10.1002/ece3.4789. ⟨http://doi.wiley.com/10.1002/ece3.4789⟩.
Qiu, B., 2001. Kuroshio And Oyashio Currents. Encyclopedia of Ocean Sciences. Elsevier,, pp. 1413–1425. https://doi.org/10.1006/rwos.2001.0350.
Quirijns, F., Poos, J., Rijnsdorp, A., 2008. Standardizing commercial CPUE data in monitoring stock dynamics: Accounting for targeting behaviour in mixed fisheries. Fish. Res. 89, 1–8. https://doi.org/10.1016/j.fishres.2007.08.016. ⟨https://linkinghub.elsevier.com/retrieve/pii/S0165783607002147⟩.
R Core Team, 2021. R: A Language and Environment for Statistical Computing. R Foundation for Statistical Computing,, Vienna, Austria. ⟨https://www.R-project.org/⟩.
Rose, G.A., Kulka, D.W., 1999. Hyperaggregation of fish and fisheries: how catch-per-unit-effort increased as the northern cod (Gadus morhua) declined. ://WOS:000085591600011 Can. J. Fish. Aquat. Sci. 56, 118–127. https://doi.org/10.1139/cjfas-56-S1-118.
Rose, G.A., Leggett, W.C., 1991. Effects of biomass range interactions on catchability of migratory demersal fish by mobile fisheries - An example of Atlantic cod (Gadus morhua). ://WOS:A1991FP95300013 Can. J. Fish. Aquat. Sci. 48, 843–848. https://doi.org/10.1139/f91-100.
Rufener, M.-C., Kristensen, K., Nielsen, J.R., Bastardie, F., 2021. Bridging the gap between commercial fisheries and survey data to model the spatiotemporal dynamics of marine species. Ecol. Appl., N./a, e02453. https://doi.org/10.1002/eap.2453 (arXiv). ⟨https://esajournals.onlinelibrary.wiley.com/doi/pdf/10.1002/eap.2453⟩.
Senina, I., Lehodey, P., Calmettes, B., Dessert, M., Hampton, J., Smith, N., Gorgues, T., Aumont, O., Lengaigne, M., Menkes, C., Nicol, S., & Gehlen, M., (2018). Impact of climate change on tropical Pacific tuna and their fisheries in Pacific Islands waters and high seas areas. Technical Report WCPFC-SC14–2018/EB-WP-01 Busan, South Korea, 8–16 August 2018.
Senina, I., Lehodey, P., Sibert, J., Hampton, J., 2020. Integrating tagging and fisheries data into a spatial population dynamics model to improve its predictive skills. Can. J. Fish. Aquat. Sci. 77, 576–593. https://doi.org/10.1139/cjfas-2018-0470. ⟨http://www.nrcresearchpress.com/doi/10.1139/cjfas-2018-0470⟩.
Senina, I., Sibert, J., Lehodey, P., 2008. Parameter estimation for basin-scale ecosystem-linked population models of large pelagic predators: Application to skipjack tuna. Prog. Oceanogr. 78, 319–335. https://doi.org/10.1016/j.pocean.2008.06.003. ⟨https://linkinghub.elsevier.com/retrieve/pii/S0079661108001171⟩.
Shono, H., & Ogura, M., (2000). The standardized skipjack cpue, including the effect of searching devices, of the japanese distant water pole and line fishery in the western central pacific ocean. Technical Report Col.Vol.Sci.Pap. ICCAT, 51(1).
Smith, M.D., Wilen, J.E., 2003. Economic impacts of marine reserves: the importance of spatial behavior. ://WOS:000185042100001 J. Environ. Econ. Manag. 46, 183–206. https://doi.org/10.1016/s0095-0696(03)00024-x.
Smith, T., & Reynolds, R., (1981). NOAA Smith and Reynolds Extended Reconstructed Sea Surface Temperature (ERSST) Level 4 Monthly Version 5 Dataset in netCDF.10.5067/ERSST-L4N50.
Stow, C.A., Jolliff, J., McGillicuddy, D.J., Doney, S.C., Allen, J.I., Friedrichs, M.A., Rose, K.A., Wallhead, P., 2009. Skill assessment for coupled biological/physical models of marine systems. J. Mar. Syst. 76, 4–15. https://doi.org/10.1016/j.

jmarsys.2008.03.011. ⟨https://linkinghub.elsevier.com/retrieve/pii/S0924796308001103⟩.
Swain, D.P., Sinclair, A.F., 1994. Fish Distribution and catchability - What is the appropriate measure of distribution. ://WOS:A1994PA36700006 Can. J. Fish. Aquat. Sci. 51, 1046–1054. https://doi.org/10.1139/f94-104.
Thorson, J.T., 2019a. Guidance for decisions using the Vector Autoregressive Spatio-Temporal (VAST) package in stock, ecosystem, habitat and climate assessments. Fish. Res. 210, 143–161. https://doi.org/10.1016/j.fishres.2018.10.013. ⟨http://www.sciencedirect.com/science/article/pii/S0165783618302820⟩.
Thorson, J.T., 2019b. Measuring the impact of oceanographic indices on species distribution shifts: The spatially varying effect of cold-pool extent in the eastern Bering Sea. Limnol. Oceanogr. 64, 2632–2645. https://doi.org/10.1002/lno.11238. ⟨https://onlinelibrary.wiley.com/doi/abs/10.1002/lno.11238⟩.
Thorson, J.T., Adams, C.F., Brooks, E.N., Eisner, L.B., Kimmel, D.G., Legault, C.M., Rogers, L.A., Yasumiishi, E.M., 2020a. Seasonal and interannual variation in spatio-temporal models for index standardization and phenology studies. ICES J. Mar. Sci. 77, 1879–1892. https://doi.org/10.1093/icesjms/fsaa074. ⟨https://academic.oup.com/icesjms/article/77/5/1879/5837191⟩.
Thorson, J.T., Barnett, L.A.K., 2017. Comparing estimates of abundance trends and distribution shifts using single- and multispecies models of fishes and biogenic habitat. ICES J. Mar. Sci. 1311–1321. https://doi.org/10.1093/icesjms/fsw193.
Thorson, J.T., Fonner, R., Haltuch, M.A., Ono, K., Winker, H., 2016. Accounting for spatiotemporal variation and fisher targeting when estimating abundance from multispecies fishery data. Canadian. J. Fish. Aquat. Sci. 1794–1807. https://doi.org/10.1139/cjfas-2015-0598.
Thorson, J.T., Kristensen, K., 2016. Implementing a generic method for bias correction in statistical models using random effects, with spatial and population dynamics examples. Fish. Res. 175, 66–74. https://doi.org/10.1016/j.fishres.2015.11.016. ⟨https://linkinghub.elsevier.com/retrieve/pii/S0165783615301399⟩.
Thorson, J.T., Maunder, M.N., Punt, E., 2020b. The development of spatio-temporal models of fishery catch-per-unit-effort data to derive indices of relative abundance. Fish. Res. 230, 105611 https://doi.org/10.1016/j.fishres.2020.105611. ⟨https://linkinghub.elsevier.com/retrieve/pii/S0165783620301284⟩.
Thorson, J.T., Shelton, A.O., Ward, E.J., Skaug, H.J., 2015. Geostatistical delta-generalized linear mixed models improve precision for estimated abundance indices for West Coast groundfishes. ://WOS:000356233800006 Ices J. Mar. Sci. 72, 1297–1310. https://doi.org/10.1093/icesjms/fsu243.
Tobler, W.R., 1970. A Computer Movie Simulating Urban Growth in the Detroit Region. Econ. Geogr. 46, 234. https://doi.org/10.2307/143141. ⟨https://www.jstor.org/stable/143141?origin=crossref⟩.
Vidal, T., Hamer, P., Escalle, L., & Pilling, G., (2020). Assessing trends in skipjack tuna abundance from purse seine catch and effort data in the WCPO. Technical Report WCPFC-SC16–2020/SA-IP-09.
Vidal, T., Muller, B., & Pilling, G., (2019a). Tropical WCPO purse seine effort creep indicators. Technical Report WCPFC-SC15–2019/MI-IP-05 Pohnpei, Federated States of Micronesia.
Vidal, T., Pilling, G., Tremblay-Boyer, L., & Usu, T., (2019b).Standardized CPUE for skipjack tuna Katsuwonus pelamis from the Papua New Guinea archipelagic purse seine fishery. Technical Report WCPFC-SC15–2019/SA-IP-05 Pohnpei, Federated States of Micronesia.
Vincent, M., Pilling, G., & Hampton, J., (2019). Stock assessment of skipjack tuna in the WCPO. Technical Report WCPFC-SC15–2019/SA-WP-05 Pohnpei, Federated States of Micronesia.
Walter, J.F., Hoenig, J.M., Christman, M.C., 2014a. Reducing Bias and Filling in Spatial Gaps in Fishery-Dependent Catch-per-Unit-Effort Data by Geostatistical Prediction, I. Methodology and Simulation. ://WOS:000348391600003 North Am. J. Fish. Manag. 34, 1095–1107. https://doi.org/10.1080/02755947.2014.932865.
Walter, J.F., Hoenig, J.M., Christman, M.C., 2014b. Reducing Bias and Filling in Spatial Gaps in Fishery-Dependent Catch-per-Unit-Effort Data by Geostatistical Prediction, II. Application to a Scallop Fishery. ://WOS:000348391600004 North Am. J. Fish. Manag. 34, 1108–1118. https://doi.org/10.1080/02755947.2014.932866.
Walters, C., 2003. Folly and fantasy in the analysis of spatial catch rate data. ://WOS:000188752800001 Can. J. Fish. Aquat. Sci. 60, 1433–1436. https://doi.org/10.1139/f03-152.
Wilberg, M.J., Thorson, J.T., Linton, B.C., Berkson, J., 2009. Incorporating time-varying catchability into population dynamic stock assessment models (Incorporating Time-Varying Catchability into Population Dynamic Stock Assessment Models). Rev. Fish. Sci. 18, 7–24. https://doi.org/10.1080/10641260903294647. ⟨https://www.tandfonline.com/doi/full/10.1080/10641260903294647⟩.
Wilen, J.E., 2004. Spatial management of fisheries. Mar. Resour. Econ. 19, 7–19.
Williams, P., Reid, C., & Ruaia, T., 2020. Overview of tuna fisheries in the WCPO, including economic conditions - 2019. Technical Report WCPFC-SC16–2020/GN-IP-01.
Xu, H., Lennert-Cody, C.E., Maunder, M.N., Minte-Vera, C.V., 2019. Spatiotemporal dynamics of the dolphin-associated purse-seine fishery for yellowfin tuna (Thunnus albacares) in the eastern Pacific Ocean. Fish. Res. 213, 121–131. https://doi.org/10.1016/j.fishres.2019.01.013. ⟨https://linkinghub.elsevier.com/retrieve/pii/S016578361930013X⟩.
Yasuda, I., Okuda, K., Hirai, M., 1992. Evolution of a Kuroshio warm-core ring–variability of the hydrographic structure. Deep Sea Res. Part A. Oceanogr. Res. Pap. 39, S131–S161. https://doi.org/10.1016/S0198-0149(11)80009-9. ⟨https://linkinghub.elsevier.com/retrieve/pii/S0198014911800099⟩.
Ye, Y.M., Dennis, D., 2009. How reliable are the abundance indices derived from commercial catch-effort standardization? ://WOS:000267874300013 Can. J. Fish. Aquat. Sci. 66, 1169–1178. https://doi.org/10.1139/f09-070.
Zhou, S., Campbell, R.A., Hoyle, S.D., 2019. Catch per unit effort standardization using spatio-temporal models for Australia's Eastern Tuna and Billfish Fishery. ICES J. Mar. Sci. https://doi.org/10.1093/icesjms/fsz034. ⟨https://academic.oup.com/icesjms/advance-article/doi/10.1093/icesjms/fsz034/5374756⟩.